HHS Public Access

Author manuscript

J Immunol. Author manuscript; available in PMC 2019 April 01.

Published in final edited form as:

J Immunol. 2018 April 01; 200(7): 2313–2326. doi:10.4049/jimmunol.1601765.

Reciprocal regulation of glycolysis-driven Th17 pathogenicity and Treg stability by Cdc42

Khalid W. Kalim[*], **Jun-Qi Yang**[*,†,1], **Yuan Li**[*,1], **Yan Meng**[*,‡], **Yi Zheng**[*], and **Fukun Guo**[*]

[*]Division of Experimental Hematology and Cancer Biology, Children's Hospital Research Foundation, Cincinnati, OH, 45229, United States of America

[†]Key Laboratory for Parasitic Disease Control and Prevention, Ministry of Health, Jiangsu Institute of Parasitic Diseases, Wuxi, Jiangsu, China

[‡]Southern Medical University, Guangzhou, Guangdong, China

Abstract

A balance between Th17 and Treg cells is important for host immunity and immune tolerance. The underlying molecular mechanisms remain poorly understood. Here we have identified Cdc42 as a central regulator of Th17/Treg balance. Deletion of Cdc42 in T cells enhanced Th17 differentiation but diminished induced Treg (iTreg) differentiation and suppressive function. Treg-specific deletion of Cdc42 decreased natural Treg (nTreg) cells but increased effector T cells including Th17 cells. Notably, Cdc42-deficient Th17 cells became pathogenic associated with enhanced glycolysis and Cdc42-deficient Treg became unstable associated with weakened glycolytic signaling. Inhibition of glycolysis in Cdc42-deficient Th17 cells diminished their pathogenicity and restoration of glycolysis in Cdc42-deficient Treg rescued their instability. Intriguingly, Cdc42 deficiency in T cells led to exacerbated wasting disease in mouse models of colitis and Treg-specific deletion of Cdc42 caused early, fatal lymphoproliferative diseases. In summary, we show that Cdc42 is a bona fide regulator of peripheral tolerance through suppression of Th17 aberrant differentiation/ pathogenicity and promotion of Treg differentiation/stability/ function involving metabolic signaling and thus Cd42 pathway might be harnessed in autoimmune disease therapy.

Keywords

Th17; Treg; Cdc42; Glycolysis; Autoimmunity; Colitis

Corresponding Author: Fukun Guo, PhD, Division of Experimental Hematology and Cancer Biology, Children's Hospital Research Foundation, 3333 Burnet Avenue, Cincinnati, OH 45229; fukun.guo@cchmc.org; telephone: 1-5138031118; fax: 1-5136363768.

[1]Equal contributions

AUTHOR CONTRIBUTIONS

K. W. K designed and performed research, analyzed data, and wrote the paper; J. Q. Y. performed research and analyzed data; Y.L. performed research and analyzed data; Y.M. performed research; Y. Z. designed research; F. G. designed research, analyzed data, contributed vital new reagents or analytical tools, and wrote the paper.

INTRODUCTION

Upon antigen recognition, naive $CD4^+$ T cells differentiate to several types of effector cells, including IFN-γ-producing T helper 1 (Th1) and IL-17-producing Th17 cells. Th17 cells, induced by the transcriptional factor RORγT, are functionally diverse. On the one hand, Th17 cells play a critical role in the clearance of extracellular bacterial and fungal infections. On the other hand, these cells can be pathogenic and induce tissue inflammation and autoimmune diseases (1). Protective, non-pathogenic Th17 cells can be generated in vitro from naïve T cells by using TGF-β and IL-6, whereas pathogenic Th17 cells can be generated by using TGF-β + IL-6 + IL-23 or IL-1β + IL-6 + IL-23 (2). It has recently been found that pathogenic Th17 cells upregulate 16 pro-inflammatory genes (e.g., T-bet, IL-23R and IL-22), while downregulate 7 regulatory genes (e.g., IL-10) (3). Th17 cells may become plastic as they can transdifferentiate to a cell subset co-expressing Th17 and Th1 cytokines and to Th1 cells (4). Th17 plasticity has been implicated in pathogenesis of inflammatory bowel diseases (IBD) (4). In line with that pathogenic Th17 cells express Th1 signature transcriptional factor T-bet, it is conceivable that Th17 pathogenicity is closely associated with their plasticity. Nonetheless, the molecular mechanisms that control Th17 pathogenicity/plasticity remain poorly defined, identification of which could allow selective suppression of pathogenic Th17 cells while sparing non-pathogenic Th17 cells.

Regulatory T cells (Treg) are the cells that maintain immune tolerance by inhibition of T cell proliferation and effector T cell function (5). Treg cell are identified by the expression of transcriptional factor Foxp3 and can be classified as natural Treg (nTreg) and induced Treg (iTreg). nTreg cells are developed from the thymus whereas iTreg cells are derived from peripheral naïve T cells (6). TGFβ has been shown to maintain nTreg in the periphery and drives iTreg differentiation (6).

The balance between Th17 and Treg is important for host immunity and immune tolerance. Loss of this balance can lead to excessive Th17-mediated immune responses and undesired autoimmunity (7, 8). It is generally considered that loss of Th17/Treg balance is attributed to altered differentiation and/or impaired Treg suppressive function (5). Nonetheless, most recent studies suggest that Treg lineage instability also contributes to imbalance between effector T (e.g. Th17) and Treg (9–16). Treg lineage instability is a phenomenon that Treg cells lose Foxp3 and acquire effector T cell functions, during which an intermediate cell population coexpressing Foxp3 and effector T cell signature genes may emerge (4, 9–13). The mechanisms underlying Treg instability are largely undetermined.

Cdc42 of the Rho family small GTPases is an intracellular signal transducer that cycles between GTP-bound active and GDP-bound inactive states (17, 18). In T cells, overexpression of constitutively active or dominant negative mutant of Cdc42 suggests that Cdc42 plays a role in T cell actin and tubulin cytoskeleton polarization, migration, and development (19–22). By genetic deletion of Cdc42 in T cells, we have recently reported that Cdc42 positively regulates naïve T cell homeostasis but negatively regulates T cell activation and Th1 cell differentiation (23, 24). In this study, we further report that Cdc42 is required for Th17/Treg balancing by negative regulation of Th17 differentiation/

pathogenicity and positive regulation of Treg differentiation/ suppressive function/stability through integrating transcriptional and metabolic signaling.

MATERIALS AND METHODS

Mice

Cdc42$^{fl/fl}$ mice were generated as described previously (25). LCK^{cre} mice and Foxp3$^{YFP\text{-}Cre}$ were purchased from The Jackson Laboratory. Cdc42$^{fl/fl}$ mice were bred with LCK^{cre} mice or Foxp3$^{YFP\text{-}Cre}$ mice in our animal facility to generate Cdc42$^{fl/fl}$LCK^{cre} mice or Cdc42$^{fl/fl}$ Foxp3$^{YFP\text{-}Cre}$ mice. RAG1$^{-/-}$ mice and BoyJ mice were obtained from the Cincinnati Children's Hospital Research Foundation Comprehensive Mouse and Cancer Core. All mice were housed under specific pathogen-free conditions in the animal facility at the Cincinnati Children's Hospital Research Foundation in compliance with the Cincinnati Children's Hospital Medical Center Animal Care and Use Committee protocols.

Antibodies, cytokines, and reagents

Antibodies for flow cytometry were obtained from BD Biosciences, eBioscience or Biolegend. Anti-CD3 (clone-145-2c11) (Cat.no. 553057) and anti-CD28 (clone-37.1) (Cat.no. 553294) were purchased from BD Biosciences. Anti-pSmad2/3 (Cat. no. 8828) and anti-Smad2/3 (Cat. no. 5678) were purchased from Cell Signaling Technology. Anti- IFN-γ and anti-IL-4 and recombinant cytokines IL-6 and IL-2 were purchased from R&D Systems. TGF-β was purchased from Peprotech. Dextran sodium sulphate (DSS) (Cat. no. 0216011050) was purchased from MP Biomedicals. 2-Deoxyglucose (2-DG) (Cat. no. D6134), Collagenase (Cat. no. C5138), Phorbol 12-myristate 13-acetate (PMA) (Cat. no. P8139), and Ionomycin (Cat. no. I0634) were purchased from sigma. IL-17A and IFN-γ ELISA sets were purchased from BD Biosciences. ELISA kits for Anti-dsDNA and Anti-Nuclear Antibody were purchased from Alpha Diagnostic International.

In vitro Th17 and iTreg differentiation

Total splenocytes were subjected to CD4$^+$ T cell isolation using CD4$^+$ T cell isolation kit (Cat. no. 130-104-454) (Miltenyi Biotech), according to the manufacturer's protocol. The MACS-sorted CD4$^+$ T cells were stained for CD4, CD62L and CD44. Naïve CD4$^+$CD62L$^+$CD44$^-$ cells were FACS-sorted and stimulated with plate bound anti-CD3 (2 μg/ml) and soluble anti-CD28 (2 μg/ml) along with either TGF-β (1 ng/ml), IL-6 (30 ng/ml), anti-IFNγ (10 μg/ml) and anti-IL-4 (10 μg/ml) for Th17 differentiation for 4 days or TGF-β (5 ng/ml), IL-2 (10 ng/ml), anti-IFNγ (10 μg/ml) and anti-IL-4 (10 μg/ml) for iTreg differentiation for 4 days. Cells were re-stimulated with PMA (5 ng/ml) and Ionomycin (50 ng/ml) along with Golgi plug (BD Biosciences) for 4 hrs and then harvested and proceeded either for intracellular staining or real-time RT-PCR.

Flow cytometry

Cells were incubated with anti-CD16/32 (2.4G2) (BD Biosciences) to block FcγR II/III, and then stained with various conjugated antibodies as indicated. BD Cytofix/Cytoperm kit (BD Biosciences) was used for intracellular staining. Stained cells were analyzed by BD LSRII,

Canto and Fortessa flow cytometer. Data were analyzed with BD FACS Diva and Flowjo software.

For BrdU incorporation assay, mice were injected i.p. with 500 μg BrdU. Two hours after injection, splenocytes were isolated and immunolabeled with anti-CD4 antibody and BrdU incorporation was analyzed by a BrdU Flow kit per manufacturer's protocol (BD Biosciences).

For cell apoptosis assay, freshly isolated splenocytes were incubated with anti-CD4 antibody for 20 min. The cells were washed, incubated with Annexin V (BD Biosciences) for 20 min, and then analyzed by flow cytometry.

Retroviral transduction of iTreg cells

FACS-sorted naïve $CD4^+CD62L^+CD44^-$ T cells were activated with plate-bound anti-CD3 and anti-CD28 along with anti-IFN-γ, anti-IL-4 and recombinant IL-2 for 24 hrs. Retroviral mock vector (pBabe-neo) or Smad2 (pBabe RFP1-Smad2 neo) (Addgene) was added to the activated T cells followed by centrifugation at 1000 g for 90 min at 32°C. After 24 hrs, another round of spin infection was performed. Cells were then cultured under iTreg polarizing condition for 3 days. After 3 days, cells were re-stimulated with PMA/Ionomycin along with Golgi Stop followed by intracellular staining and flow cytometry analysis of $Foxp3^+$ cells.

Quantitative real-time RT-PCR analysis

Total RNA was extracted with RNeasy mini kit from QIAGEN. Isolated RNA was converted to cDNA by using High-Capacity cDNA Reverse Transcription Kit (Applied Biosystems). Real-time RT-PCR was performed with Platinum®SYBR®Green qPCR SuperMix-UDG with ROX and measured on StepOnePlus™ Real-Time PCR System (Applied Biosystem). Data were normalized to 18S rRNA.

Primer sequences:

1. RORγT Fwd – 5′ TTTGGAACTGGCTTTCCATC 3′ Rev- 5′ AAGATCTGCAGCTTTTCCACA 3′
2. DUSP2 Fwd – 5′ CGGTTTCAAAAGCTTCCAGA 3′ Rev- 5′ CAGGTAGGGCAAGATTTCCA 3′
3. IL-23R Fwd- 5′ TTCAGATGGGCATGAATGTTTCT 3′ Rev - 5′ CCAAATCCGAGCTGTTGTTCTAT 3′
4. T-Bet Fwd - 5′ CCTCTTCTATCCAACCAGTATC 3′ Rev – 5′ CTCCGCTTCATAACTGTGT 3′
5. IL-22 Fwd – 5′ GTGAGAAGCTAACGTCCATC 3′ Rev - 5′ GTCTACCTCTGGTCTCATGG 3′
6. HIF1α Fwd – 5′ AGCTTCTGTTATGAGGCTCACC 3′ Rev - 5′ TGACTTGATGTTCATCGTCCTC 3′

7. PDK-1 Fwd – 5′ GGACTTCGGGTCAGTGAATGC 3′ Rev - 5′ TCCTGAGAAGATTGTCGGGGA 3′
8. PGM-1 Fwd – 5′ CAGAACCCTTTAACCTCTGAGTC 3′ Rev - 5′ CGAGAAATCCCTGCTCCCATAG 3′
9. Smad2 Fwd – 5′ CTCCAGTCTTAGTGCCTCGG 3′ Rev - 5′ AACACCAGAATGCAGGTTCC 3′
10. Smad3 Fwd – 5′ TTCACTGACCCCTCCAACTC 3′ Rev - 5′ CTCCGATGTAGTAGAGCCGC 3′
11. HMGCR Fwd- 5′ TGGTCCTAGAGCTTTCTCGTGAA Rev- 5′ GGACCAAGCCTAAAGACATAATCATC
12. FASN Fwd – 5′ TGGGTTCTAGCCAGCAGAGT Rev- 5′ ACCACCAGAGACCGTTATGC 3′
13. HK2 Fwd – 5′ TGATCGCCTGCTTATTCACGG 3′ Rev – 5′ AACCGCCTAGAAATCTCCAGA 3′
14. Cdc42 Fwd – 5′ TGCAGGGCAAGAGGATTATG 3′ Rev - 5′ GATGGAGAGACCACTGAGAAA 3′
15. 18S Fwd - 5′ GTAACCCGTTGAACCCCATT 3′ Rev - 5′ CCATCCAATCGGTAGTAGCG 3′
16. AldoC Fwd – 5′ AATTGGGGTGGAGAACACTG 3′ Rev - 5′ TGTCAACCTTGATGCCTACG 3′
17. Slc2a Fwd – 5′ CAGTTCGGCTATAACACTGGTG 3′ Rev - 5′ GCCCCCGACAGAGAAGATG 3′
18. Foxp3 Fwd – 5′ GGTACACCCAGGAAAGACAG 3′ Rev - 5′ ATCCAGGAGATGATCTGCTTG 3′
19. HMGCS Fwd – 5′ CAGGGTCTGATCCCCTTTG 3′ Rev - 5′ CAGAGAACTGTGGTCTCCAGGT 3′
20. Sqle Fwd – 5′ GCCTCTCAGAATGGTCGTCT 3′ Rev - 5′ CGCATCTCCCAGAATAAGGA 3′
21. Acaca Fwd – 5′ GGCCAGTGCTATGCTGAGAT 3′ Rev - 5′ CCAGGTCGTTTGACATAATGG 3′
22. IL-4 Fwd – 5′ AGATCATCGGCATTTTGAACG 3′ Rev - 5′ TTTGGCACATCCATCTCCG 3′
23. IFN-γ Fwd – 5′ GATGCATTCATGAGTATTGCCAAGT 3′ Rev - 5′ GTGGACCACTCGGATGAGCTC 3′
24. GATA3 Fwd – 5′ AGAACCGGCCCCTTATCAA 3′ Rev - 5′ AGTTCGCGCAGGATGTCC 3′

25. DNMT3a Fwd – 5′ ACTTGGAGAAGCGGAGTGAA 3′ Rev - 5′ GGATTCGATGTTGGTCTGCT 3′

26. Tet1 Fwd – 5′ ATCATTCCAGACCGCAAGAC 3′ Rev - 5′ AATCCATGCAACAGGTGACA 3′

Immunoblot analysis

Cells were extracted using RIPA lysis buffer (1× PBS, 1% Nonidet P-40, 0.5% sodium deoxycholate, 0.1% SDS, 1 mM phenyl methyl sulfonyl fluoride, and protease inhibitors). Lysates were resolved by SDS-PAGE, electrophoretically transferred onto PVDF membrane (Bio-Rad), and probed with the indicated antibodies. The bands were visualized with the enhanced chemiluminescence system (Thermo Scientific).

DSS- induced colitis

Colitis was induced in 8–10 week old mice by giving the mice 2.2% DSS (M.W. 36,000–50,000) in drinking water for 5 days followed by normal water for another 5 days. Mouse body weight was measured daily. The mice were sacrificed after 10 days and the spleen, mLN and colon were harvested for intracellular cytokine and Foxp3 staining.

Naïve T-cell transfer model of colitis

Colitis was induced by injecting intraperitoneally 0.6×10^6 of FACS-sorted naïve $CD4^+CD62L^+CD44^-$ cells into age- and sex-matched $RAG1^{-/-}$ mice. Mice were weighed daily and sacrificed upon losing 20–25% of initial body weight. The spleen, mLN and colon were harvested for intracellular cytokine and Foxp3 staining.

Isolation of lamina propria lymphocytes

The colon was harvested from the colitis mouse models into harvesting media (HBSS (Hanks-balanced salt solution)) with addition of glucose and 2% FBS. The colon was then opened longitudinally and cut into small pieces and incubated with constant stirring in harvesting media with addition of DTT and EDTA at 37 °C for 30 min. The colon pieces were then washed twice with harvesting media with addition of EDTA and digested with collagenase in HBSS with addition of glucose and 5% FBS at 37 °C for 30 min. The digested colon was then filtered with 70 μm cell strainer and centrifuged at 1500 rpm at 4 °C for 5 min. The pellets were dissolved in 8 ml of 40% percoll and slowly layered over 5 ml of 80% percoll in a 15 ml falcon tube. The falcon tube was then centrifuged at 2000 rpm at 4 °C for 20 min with acceleration of 3 and deceleration of 2. The lamina propria lymphocytes were carefully removed from the interface between 40% percoll and 80% percoll. The isolated lamina propria lymphocytes were washed twice with complete RPMI T-cell medium, cultured with anti-CD3 (4 μg/ml) and anti-CD28 (8 μg/ml) for 5 hrs in the presence of Golgi plug for the last 4, and then proceeded for intracellular staining.

Histopathological analysis

Tissues were sectioned, fixed in 4% formaldehyde solution, embedded in paraffin, and stained with hematoxylin and eosin. The sections were analyzed by light microscopy from

Fisher Scientific Moticam at 20X magnification at room temperature. The images were acquired by using the software Motic Images Plus 2.0.

Metabolic assay

Th17 or iTreg cells were resuspended in assay medium (pH 7.4) (Sigma) containing 2 mM L-Glutamine, plated onto XF24 cell culture plates pre-coated with Cell Tak (BD Biosciences), and incubated without CO_2 at 37°C. Extracellular acidification rate (ECAR), an indicator of aerobic glycolysis, was measured using the Seahorse XF24 Analyzer (Seahorse Bioscience) in the presence of the glycolysis substrate glucose (10 mM).

In vivo suppression assay

$CD25^{hi}IL\text{-}7R^{lo}$ iTregs were sorted by FACS. 3×10^5 iTregs were mixed with 6×10^5 naïve $CD4^+CD62L^+CD44^-$ cells from congenic BoyJ mice and transferred i.p. into age- and sex-matched $RAG1^{-/-}$ mice. The recipient mice were weighed every other day for the first week and every day thereafter. The mice were sacrificed and the colon was isolated for histopathological analysis and intracellular cytokine staining.

Bisulfite pyrosequencing of methylation of Foxp3 enhancer

A total of 200ng genomic DNA was subjected to sodium bisulfite treatment and purified using the EZ DNA methylation-Gold Kit (Zymo research, Irvine, CA, USA) according to the manufacturer's specifications. Two rounds of standard PCR amplification reaction were performed to amplify targeted gene fragment at an annealing temperature of 50°C before being subjected to pyrosequencing. The generated pyrograms were automatically analyzed using PyroMark analysis software (Qiagen, Valencia, CA, USA). The pyrosequencing assay was validated using SssI-treated human genomic DNA as a 100% methylation control and human genomic DNA amplified by GenomePlex® Complete WGA kit (Sigma, St. Louis, MO, USA) as 0% methylation control.

Primers used for Bisulfite Pyrosequencing are as follows:

mFoxp3_assay1_NF: TTTGTGTTTTTGAGATTTTAAAATT

mFoxp3_assay1_NR: /5Biosg/AAAAATAACTAATCTATCCTATAACC

mFoxp3_assay1_LF: TATTTTTTTGGGTTTTGGGATATTA

mFoxp3_assay1_LR: ACAAATAATCTACCCCACAAATTTC

mFoxp3_assay1_S2: GGGTTTTTTTGGTATTTAAGAAAG

mFoxp3_assay1_S3: GGGTTTTGTATGGTAGTTAGATGG

mFoxp3_assay1_S4: AGTATTTATATTATTTTATTTGGG

mFoxp3_assay2_NF: GGTTATAGGATAGATTAGTTATTTTT

mFoxp3_assay2_NR: /5Biosg/CCAACTTCCTACACTATCTATTAAAAC

mFoxp3_assay2_LF: TTTATATTATTTTATTTGGGTTTATT

mFoxp3_assay2_LR: ATAACTATATAATACATCAATACATTCTCA

mFoxp3_assay2_S2: GTTTTTTTTTTTTTTTTTTGTTG

mFoxp3_assay2_S3: GGTTGTGATAATAGGGTTTAGATGTAG

mFoxp3_assay2_S4: GTTTTTAAGAAATAGTTAAATAGG

Competitive bone marrow transplantation

A total of 2×10^6 donor bone marrow cells were mixed with recipient bone marrow cells at 1:1 ratio and injected into the tail veins of lethally irradiated BoyJ mice. Eight weeks after transplantation, the chimeric mice were sacrificed, and $CD45.2^+$ thymocytes and splenic T cells derived from donor bone marrow cells were analyzed.

Statistical analysis

All the statistics were performed with the two-tailed student's t-test. Data were expressed as mean ± SD. $p \leq 0.05$ was considered significant.

RESULTS

Cdc42 restrains aberrant Th17 cell differentiation and Th17 cell pathogenicity through repression of glycolysis

To study the role of Cdc42 in Th17 cell differentiation, Cdc42-deficient and wild type (WT) $CD4^+$ T cells were isolated from mice bearing Cdc42 deletion in T cells ($Cdc42^{fl/fl}Lck^{Cre}$) and WT mice ($Cdc42^{+/+}Lck^{Cre}$), respectively, and cultured under non-pathogenic Th17 differentiation condition (TGFβ + IL-6). We found that Cdc42 deficiency significantly increased IL-17 production upon 2 day culture (Supplemental Fig. 1A, 1B) or PMA/ionomycin restimulation at day 5 (Fig. 1A), suggesting that Cdc42 deficiency causes aberrant Th17 cell differentiation. Consistently, Cdc42-deficient Th17 cells expressed higher levels of RORγT (Fig. 1B), a key transcriptional factor for Th17 induction (1). Noting that RORγT expression is controlled by Stat3 (1), Stat3 activity was markedly enhanced in Cdc42-deficient Th17 cells with or without IL-6 restimulation (Fig. 1C). Conversely, DUSP2, a phosphatase inactivating Stat3 (26), was downregulated in Th17 cells lacking Cdc42 (Fig. 1D). Interestingly, under non-pathogenic Th17 differentiation condition, Cdc42 deficiency resulted in emergence of $IL\text{-}17^+IFN\text{-}\gamma^+$ cells and $IFN\text{-}\gamma^+$ Th1 cells and increased secretion of IFN-γ (Fig. 1A; supplemental Fig. 1C), suggesting that ablation of Cdc42 converts non-pathogenic Th17 cells to pathogenic Th17 cells. In support, we found that IL-23R, T-bet and IL-22, three important signature genes of pathogenic Th17 cells (3), were substantially elevated in Cdc42-deficient Th17 cells (Fig. 1E). These data suggest that Cdc42 restrains aberrant Th17 differentiation and Th17 pathogenicity.

Glycolysis has recently been shown to be essential for Th17 cell differentiation (27). We found that Cdc42 deletion led to an increased glycolysis in Th17 cells (Fig. 2A). In agreement with this, Hif1α, PDK1, PGM1, HK2, AldoC, and Slc2a that indirectly (e.g. Hif1α, PDK1, PGM1, Slc2a) or directly (e.g. HK2, AldoC) regulate glycolysis were upregulated in Cdc42-deficient Th17 cells (Fig. 2B). Importantly, inhibition of glycolysis by 2-DG reversed IL-17 expression in pathogenic Cdc42-deficient Th17 cells (Fig. 2C). Of note, 2-DG also suppressed IL-17 expression in non-pathogenic WT Th17 cells (Fig. 2C),

supporting the essential role of glycolysis in Th17 cell differentiation. Interestingly, upon 2-DG treatment, IL-17 in Cdc42-deficient Th17 cells was decreased to the comparable levels to that in WT Th17 cells but not to that in 2-DG-treated WT Th17 cells (Fig. 2C). Furthermore, 2-DG treatment reduced the transdifferentiation of Cdc42-deficient Th17 cells to IL-17$^+$IFN-γ^+ cells and IFN-γ^+ cells (Fig. 2C). These data suggest that inhibition of glycolysis diminished aberrant differentiation and pathogenicity of Cdc42-deficient Th17 cells. Lipid metabolism may play a role in Th17 differentiation (28). Consistent with the increased Th17 differentiation, we found that Cdc42 deficiency upregulated lipid metabolism regulators HMGCS, FASN and SQLE in Th17 cells (Supplemental Fig. 1D).

Because Cdc42-deficient Th17 cells became pathogenic, we next examined whether they had functional impact in vivo on colitis development in which pathogenic Th17 cells play an important role (4, 29). As expected, Cdc42-deficient mice lost more weight compared to WT mice, upon treatment with dextran sulfate sodium (DSS) (Fig. 3A), a well-known regimen to model human colitis in mice (30). This is associated with more IL-17$^+$ cells in the colon (Fig. 3B). Furthermore, in support of a recent report that Th17 cells give rise to Th1 cells in the pathogenesis of colitis (29), we found increased IFN-γ^+ cells in DSS-treated Cdc42-deficient mice (Fig. 3B). To substantiate these results, we adopted a naïve T cell transfer-induced mouse model of colitis in which naive CD4$^+$ T cells are transferred into Rag1$^{-/-}$ mice to induce colitis (30). As shown in Fig. 3C, both WT and Cdc42 knockout naïve T cells induced weight loss in Rag1$^{-/-}$ mice starting at about two and half weeks after cell transfer. Nonetheless, Rag1$^{-/-}$ mice receiving Cdc42 knockout naïve T cells suffered from significantly more weight loss 5 weeks later. The severe wasting disease in the mice receiving Cdc42 knockout naïve T cells is associated with increased IL-17A$^+$, IFN-γ^+, and IL-17A$^+$IFN-γ^+ cells in the spleen and/or mesenteric lymph nodes (MLN) (Fig. 3D). Surprisingly, IL-17$^+$, IFN-γ^+ and IL-17A$^+$IFN-γ^+ cells in lamina propria were decreased or tended to decrease (Fig. 3D), which might reflect a negative feedback effect. Taking together, these results suggest that Cdc42 prevents colitis development through suppression of Th17 differentiation and pathogenicity.

Cdc42 promotes iTreg cell differentiation, stability and suppressive function

We next examined the effect of Cdc42 deficiency on iTreg differentiation. As shown in Fig. 4A, deletion of Cdc42 dampened iTreg differentiation as Foxp3$^+$ cells were considerably reduced when Cdc42-deficient CD4$^+$ T cells were differentiated with TGF-β and IL-2. Interestingly, under iTreg differentiation condition, there was a significant increase in Foxp3$^+$IL-17$^+$, IL-17$^+$, IL-17$^+$IFN-γ^+, and IFN-γ^+ cells in the absence of Cdc42 (Fig. 4A, 4B), suggesting that Cdc42 deficiency caused iTreg instability. In addition, Cdc42 deficiency-induced defect in iTreg differentiation was mirrored in vivo. Thus, DSS-treated Cdc42-deficient mice and Rag1$^{-/-}$ mice transferred with naïve CD4$^+$ Cdc42-deficient T cells showed less Foxp3$^+$ cells in their lamina propria, spleen and/or mLN (Fig. 4C, 4D).

Mechanistically, Cdc42 deficiency led to an attenuated activation and mRNA/protein expression of transcriptional factors Smad2 and Smad3 that are known to be induced by TGF-β and are important for Foxp3 expression in iTreg (5) (Fig. 5A, 5B). Reconstitution of Smad2 into Cdc42-deficient iTreg cells partially restored their differentiation (Fig. 5C;

Supplemental Fig. 1E, 1F), suggesting that the decreased Smad2 expression in Cdc42-deficient iTreg contributes to the impaired differentiation and that Smad2 is necessary for Cdc42 to regulate iTreg differentiation. Noting that overexpression of Smad2 in WT iTreg did not enhance iTreg differentiation (Fig. 5C; Supplemental Fig. 1E, 1F), it appears that Smad2 is not sufficient to promote iTreg differentiation. In contrast to its inhibitory effect on Smad2/3 expression/activation, Cdc42 deficiency in iTreg had no effect on IL-2-induced Stat5 activation (Fig. 5D). Lipid metabolism and glycolysis have been indicated in Treg differentiation and/or stability (11, 12, 31–34). We found that although Cdc42 deficiency in iTreg cells had no effect on the expression of lipid metabolism enzymes HMGCS and ACACA, it inhibited HMGCR and FASN expression (Fig. 5E), suggesting a defective lipid metabolism in Cdc42-deficient iTreg cells. Cdc42 deficiency also dampened glycolysis and the expression of glycolysis mediators Hif1α and HK2 in iTreg (Fig. 5F, 5G). Importantly, Cdc42 deficiency-induced increase in $Foxp3^{+}IL\text{-}17^{+}$ cells was abolished by addition of glycolysis-derived pyruvate into culture medium of Cdc42-deficient iTreg cells (Fig. 5H), an approach mimicking restoration of glycolysis through bypassing the intermediate steps of glycolysis (35). In contrast, Cdc42 deficiency-induced decrease in $Foxp3^{+}$ cells was not reversed by addition of pyruvate (Fig. 5H). These data suggest that Cdc42-mediated glycolysis is important for iTreg stability but not differentiation. To further demonstrate the importance of glycolysis in maintaining iTreg stability, we treated WT iTreg cells with 2-DG and found that 2-DG caused iTreg instability as evidenced by reduced $Foxp3^{+}$ cells and concomitantly increased $IL\text{-}17^{+}$ cells (Fig. 5I). Collectively, our data suggest that Cdc42 is required for iTreg differentiation and stability through coordinating transcriptional and metabolic signaling.

We then evaluated functional capacity of Cdc42-deficient iTreg cells. To this end, WT or Cdc42-deficient iTreg cells were transferred together with congenic naïve $CD4^{+}$ T cells from BoyJ mice into $Rag1^{-/-}$ mice. We found that while WT iTreg abolished naïve T cell transfer-induced weight loss, Cdc42-deficient iTreg cells failed to suppress the wasting disease (Fig. 6A). The loss of function of Cdc42-deficient iTreg cells in control of colitis was associated with their inability to suppress infiltration of inflammatory cells (Fig. 6B), particularly IL-17- and IFN-γ-producing cells (Fig. 6C), into the colon.

Cdc42 promotes nTreg stability and controls autoimmune diseases

The observation that Cdc42 deficiency caused an enhanced Th17 cell differentiation and pathogenicity in vitro and in induced colitis models prompted us to examine whether Th17 cells were spontaneously developed in steady-state $Cdc42^{fl/fl}Lck^{Cre}$ mice. Indeed, $Cdc42^{fl/fl}Lck^{Cre}$ mice had more IL-17-producing cells compared to control mice (Supplemental Fig. 1G). And these cells appeared to be pathogenic as they inclined to develop to IFN-γ-producing cells (Supplemental Fig. 1G). Brief restimulation of splenocytes from $Cdc42^{fl/fl}Lck^{Cre}$ mice in vitro also induced more $IL\text{-}17^{+}$ cells than that from WT mice (Supplemental Fig. 1H). However, $Cdc42^{fl/fl}Lck^{Cre}$ mice did not appear to have spontaneous autoimmune diseases (data not shown) and apparent pathological abnormalities in the spleen, kidney, liver and colon (Supplemental Fig. 1I). This is likely due to a compensatory increase in the frequency but not the absolute numbers of nTreg cells (Supplemental Fig. 1J, 1K) (24).

The compensatory increase in nTreg cells in $Cdc42^{fl/fl}Lck^{Cre}$ mice precludes us from studying nTreg autonomous role of Cdc42 in these mice. To circumvent this hurdle, we achieved Treg cell-specific deletion of Cdc42 by crossing $Cdc42^{fl/fl}$ mice with $Foxp3^{YFP\text{-}Cre}$ mice. The resultant $Cdc42^{fl/fl}Foxp3^{YFP\text{-}Cre}$ mice showed effective Cdc42 deletion in their nTreg cells (Fig. 7A; Supplemental Fig. 2A for nTreg flow-sorting strategy). Strikingly, $Cdc42^{fl/fl}Foxp3^{YFP\text{-}Cre}$ mice were small in size, lacked mobility, and developed a hunched posture, crusting of the ears, eyelids and tail, and skin ulceration, before they became moribund within about 3–5 weeks after birth (Fig. 7B and data not shown). Moreover, the mice showed splenomegaly and lymphadenopathy (Fig. 7C), massive leukocyte infiltration and/or distorted architecture in the colon, kidney, lung, and skin (Fig. 7D), and increased autoantibodies (e.g. anti-dsDNA, ANA) (Fig. 7E). Such severe phenotypes are reminiscent of that observed in mice with the scurfy mutation of Foxp3 gene and mice depleted of Treg cells (36–38). The systemic inflammatory diseases in $Cdc42^{fl/fl}Foxp3^{YFP\text{-}Cre}$ mice are associated with altered T cell homeostasis. As such, the mice showed more activated T cells ($CD62L^{lo}CD44^{hi}$) in their $CD4^+$ and $CD8^+$ compartments (Fig. 7F) and more effector T cells (e.g. IL-17-producing Th17, IFN-γ-producing Th1, IL-4-producing Th2) (Fig. 7G). Consistently, these mice had increased cells expressing Th1 and Th2 signature transcriptional factor T-bet and GATA3, respectively (Supplemental Fig. 2B). On the other hand, $Cdc42^{fl/fl}Foxp3^{YFP\text{-}Cre}$ mice had less $Foxp3^+$ cells (Fig. 7H), suggesting that the immune activation in $Cdc42^{fl/fl}Foxp3^{YFP\text{-}Cre}$ mice is likely due to the decreased nTreg cells.

To explore the mechanisms underlying the loss of nTreg cells in $Cdc42^{fl/fl}Foxp3^{YFP\text{-}Cre}$ mice, we measured nTreg cell proliferation and apoptosis. nTreg cells from $Cdc42^{fl/fl}Foxp3^{YFP\text{-}Cre}$ mice showed less BrdU incorporation (Fig. 8A) and more Annexin V staining (Fig. 8B; Supplemental Fig. 2C), compared to that from control $Cdc42^{+/+}Foxp3^{YFP\text{-}Cre}$ mice, suggesting that Treg-specific deletion of Cdc42 dampens nTreg cell proliferation and survival, which likely contributes to the reduction in nTreg cells in $Cdc42^{fl/fl}Foxp3^{YFP\text{-}Cre}$ mice.

The impaired nTreg homeostasis in $Cdc42^{fl/fl}Foxp3^{YFP\text{-}Cre}$ mice could also have resulted from nTreg instability. Indeed, $Cdc42^{fl/fl}Foxp3^{YFP\text{-}Cre}$ nTreg cells became plastic and gained effector T cell programs as they produced more effector T cell cytokines IL-17, IFN-γ and IL-4 and expressed more effector T cell transcriptional factors RORγT, T-bet and GATA3 than did by $Cdc42^{+/+}Foxp3^{YFP\text{-}Cre}$ nTreg cells (Fig. 8C, Supplemental Fig. 3A–D). Moreover, $Cdc42^{fl/fl}Foxp3^{YFP\text{-}Cre}$ nTreg cells had lower expression of Foxp3, although they exhibited intact CD25 expression (Fig. 8D). And in vitro culture of purified $Cdc42^{fl/fl}Foxp3^{YFP\text{-}Cre}$ and $Cdc42^{+/+}Foxp3^{YFP\text{-}Cre}$ nTreg cells with IL-2 (39) found that Cdc42 deficiency inhibited IL-2-induced expansion of nTreg cells and diminished Foxp3 expression (Fig. 8E). As reduced Foxp3 expression is known to convert Treg cells to effector T cells (40), we next examined if Cdc42 deficiency caused conversion of $Cdc42^{fl/fl}Foxp3^{YFP\text{-}Cre}$ nTreg cells to effector T cells. To this end, we cultured purified $Cdc42^{fl/fl}Foxp3^{YFP\text{-}Cre}$ and $Cdc42^{+/+}Foxp3^{YFP\text{-}Cre}$ nTreg cells in vitro with IL-6/IL-1 or IL-12 (10). We found that $Cdc42^{fl/fl}Foxp3^{YFP\text{-}Cre}$ nTreg cells were more susceptible than $Cdc42^{+/+}Foxp3^{YFP\text{-}Cre}$ nTreg cells to convert to IL-17-producing effector T cells upon IL-6/IL-1 culture (Fig. 8F) or IFN-γ-producing effector T cells upon IL-12 culture (Fig. 8G). In support of the increased transdifferentiation capacity of $Cdc42^{fl/fl}Foxp3^{YFP\text{-}Cre}$ nTreg cells,

we detected Cdc42 knockout allele in $CD4^+Foxp3^-$ non-Treg cells from $Cdc42^{fl/fl}Foxp3^{YFP\text{-}Cre}$ mice (Fig. 8H). Since $Foxp3^{YFP\text{-}Cre}$ presumably induces gene deletion specifically in Treg cells, the appearance of Cdc42 deletion in $Foxp3^-$ population suggests that these Cdc42-deficient non-Treg cells are converted from Cdc42-deficient nTreg cells. Treg activation has recently been shown to lead to their instability (41). Consistently, $Cdc42^{fl/fl}Foxp3^{YFP\text{-}Cre}$ nTreg cells upregulated their activation/functional markers CD44, CD69, GITR, PD-1 and CTLA-4 with concomitant downregulation of CD62L (Fig. 8I, 8J). Hypomethylation of the CNS2 region in the Foxp3 enhancer is important for maintenance of Foxp3 expression and thus Treg stability (10, 12). As reported (10, 12, 42), $CD4^+$ naïve and activated T cells from $Cdc42^{+/+}Foxp3^{YFP\text{-}Cre}$ mice showed hypermethylation and nTreg cells from $Cdc42^{+/+}Foxp3^{YFP\text{-}Cre}$ mice showed hypomethylation in all of the 14 methylation sites in the CNS2 region of the Foxp3 gene. In agreement with the loss of Foxp3 expression and instability, nTreg cells from $Cdc42^{fl/fl}Foxp3^{YFP\text{-}Cre}$ mice showed significantly more methylation in these methylation sites, compared to $Cdc42^{+/+}Foxp3^{YFP\text{-}Cre}$ nTreg cells (Fig. 8K), which is associated with upregulated DNMT3A, a DNA methyltransferase, but not TET1, a DNA demethylase (Supplemental Fig. 3E). Lastly, Cdc42 deficiency in nTreg cells dampened signaling involved in lipid metabolism (Supplemental Fig. 3F) and glycolysis (Supplemental Fig. 3G) that have been implicated in regulating Treg stability (11). Importantly, while Cdc42 deficiency enhanced IL-12-induced transdifferentiation of nTreg to IFN-γ-producing effector T cells, this effect of Cdc42 deficiency was partially reversed by glycolysis-derived pyruvate (Supplemental Fig. 3H). Collectively, our data suggest that Cdc42 deficiency destabilizes nTreg cells, leading to their transdifferentiation to effector T cells.

As inflammatory disorders may impair Treg stability (43–45), the instability of $Cdc42^{fl/fl}Foxp3^{YFP\text{-}Cre}$ nTreg cells could be due to the severe inflammation in $Cdc42^{fl/fl}Foxp3^{YFP\text{-}Cre}$ mice. To test this, we analyzed $Cdc42^{fl/fl}Foxp3^{YFP\text{-}Cre/+}$ female mice that are heterozygous for $Foxp3^{YFP\text{-}Cre}$ and didn't show overt inflammation (data not shown). Due to the X chromosome-linked nature of and random X chromosome inactivation by $Foxp3^{YFP\text{-}Cre}$ knock-in transgene, $Foxp3^{YFP\text{-}Cre/+}$ female mice should maintain 50% of $Foxp3^+YFP^+$ nTreg cells and 50% of $Foxp3^+YFP^-$ nTreg cells (14). This was the case in $Cdc42^{+/+}Foxp3^{YFP\text{-}Cre/+}$ female mice in which $Foxp3^+YFP^+$:$Foxp3^+YFP^-$ cells were approximately 1:1 (Fig. 9A; Supplemental Fig. 4A for gating strategy). However, the ratio of $Foxp3^+YFP^+$ vs. $Foxp3^+YFP^-$ cells in $Cdc42^{fl/fl}Foxp3^{YFP\text{-}Cre/+}$ female mice was significantly reduced (Fig. 9A). BrdU incorporation and active caspase 3 staining assays revealed decreased proliferation and increased apoptosis in $Foxp3^+YFP^+$ cells from $Cdc42^{fl/fl}Foxp3^{YFP\text{-}Cre/+}$ female mice, compared to that in $Foxp3^+YFP^+$ cells from $Cdc42^{+/+}Foxp3^{YFP\text{-}Cre/+}$ female mice (Fig. 9B, 9C), which might contribute to the decreased ratio of $Foxp3^+YFP^+$ vs. $Foxp3^+YFP^-$ cells in $Cdc42^{fl/fl}Foxp3^{YFP\text{-}Cre/+}$ female mice. Since $Foxp3^+YFP^+$ nTreg cells from $Cdc42^{fl/fl}Foxp3^{YFP\text{-}Cre/+}$ female mice presumably lack Cdc42 expression and $Foxp3^+YFP^-$ nTreg cells from the same mice express Cdc42, our data suggest that Cdc42-deficient $Foxp3^+YFP^+$ nTreg cells were outcompeted by Cdc42-sufficient $Foxp3^+YFP^-$ nTreg cells in $Cdc42^{fl/fl}Foxp3^{YFP\text{-}Cre/+}$ female mice. The uncompetitiveness of $Foxp3^+YFP^+$ nTreg cells in $Cdc42^{fl/fl}Foxp3^{YFP\text{-}Cre/+}$ female mice is associated with their instability as evidenced by increased expression of Th17, Th1 and Th2

cytokines IL-17, IFN-γ and IL-4, respectively (Fig. 9D), decreased expression of Foxp3 (Fig. 9E), and increased expression of Treg activation/functional markers GITR, PD-1, CTLA4, and ICOS (Fig. 9F), compared to $Foxp3^{+}YFP^{-}$ nTreg cells from the same mice. The instability of Cdc42-deficient nTreg cells in non-inflammatory $Cdc42^{fl/fl}Foxp3^{YFP\text{-}Cre/+}$ female mice suggests that the instability of Cdc42-deficient nTreg cells in $Cdc42^{fl/fl}Foxp3^{YFP\text{-}Cre}$ mice is not due to continuing inflammation but a cell intrinsic effect. In further support of this, a competitive bone marrow transplantation assay found that the spleen of recipient mice of $Cdc42^{fl/fl}Foxp3^{YFP\text{-}Cre}$ bone marrow had less donor-derived nTreg cells but more $Foxp3^{+}IFN\text{-}\gamma^{+}$ and $Foxp3^{+}IL\text{-}4^{+}$ cells (Fig. 9G).

The reduction in nTreg cells in $Cdc42^{fl/fl}Foxp3^{YFP\text{-}Cre}$ mice could also have been an outcome of impaired nTreg differentiation in the thymus. To test this, we analyzed thymocyte development in $Cdc42^{fl/fl}Foxp3^{YFP\text{-}Cre}$ mice. We found that while $Cdc42^{fl/fl}Foxp3^{YFP\text{-}Cre}$ mice had very small thymus (Supplemental Fig. 4B) and defective thymocyte development (e.g. decreased frequency of $CD4^{+}CD8^{+}$ thymocytes; increased frequency of $CD4^{-}CD8^{-}$, $CD4^{+}$ and $CD8^{+}$ thymocytes) (Supplemental Fig. 4C), the frequency of nTreg cells was increased (Supplemental Fig. 4D). Nonetheless, Foxp3 expression was not altered (Fig. 10A). These data suggest that Cdc42 deficiency has no effect on nTreg differentiation and that the altered thymocyte development likely results from the severe inflammation and the increased frequency of nTreg cells might be a proportional increase resulting from the increased frequency of $CD4^{+}$ thymocytes. In support, non-inflammatory $Cdc42^{fl/fl}Foxp3^{YFP\text{-}Cre/+}$ female mice had normal thymocyte development (data not shown) and normal ratio of $Foxp3^{+}YFP^{+}$ vs. $Foxp3^{+}YFP^{-}$ cells in the thymus (Fig. 10B). Furthermore, a competitive bone marrow transplantation assay found that the thymus of recipient mice of $Cdc42^{fl/fl}Foxp3^{YFP\text{-}Cre}$ bone marrow had normal frequency of donor-derived $Foxp3^{+}$ cells showing normal Foxp3 expression (Fig. 10C, 10D)

DISCUSSION

A delicate balance between effector T cells and Treg cells is important for mounting protective immune responses to foreign antigens without losing immune tolerance to self-antigens. Understanding the molecular mechanisms by which this balance is regulated is thus of paramount importance. In the present study, we demonstrate that Cdc42 is pivotal for maintaining Th17/Treg balance. This conclusion is supported by several observations: (1) genetic deletion of Cdc42 in T cells enhances Th17 differentiation but diminishes iTreg differentiation in culture under Th17 differentiation condition and iTreg differentiation condition, respectively; (2) Under Th17 differentiation condition, Cdc42 deficiency impairs the generation of $Foxp3^{+}$ cells (data not shown), whereas under iTreg differentiation condition, Cdc42 deficiency increases IL-17-producing cells; (3) $Rag1^{-/-}$ mice transferred with Cdc42-deficient naïve T cells show increased Th17 cells but decreased iTreg cells, compared to that transferred with WT naïve T cells; and (4) Treg-specific Cdc42 deletion leads to decreased nTreg cells but increased Th17 cells. Along with our previous finding that Cdc42 deficiency enhances Th1 cell differentiation (24), this study also suggests that Cdc42 plays an important role in maintaining the balance between Treg and Th1 or Th2 cells.

Cdc42-deficient Th17 cells become pathogenic, which is attributed to increased glycolysis, because inhibition of glycolysis by 2-DG in Cdc42-deficient Th17 cells suppresses aberrant IL-17 and IFN-γ production. Interestingly, 2-DG-treated Cdc42-deficient Th17 cells still show WT level of IL-17 production, whereas 2-DG-treated WT Th17 cells has decreased IL-17 production as previously reported (27). It thus appears that while glycolysis promotes Th17 differentiation, Cdc42 controls the magnitude of glycolysis to prevent aberrant/pathogenic Th17 cell differentiation. Noting that Cdc42-deficient Th17 cells upregulate Hif1α, deletion of which has been shown to inhibit Th17 glycolysis and differentiation (27), it is plausible that Cdc42 restrains glycolysis and its regulated Th17 differentiation through suppression of Hif1α expression. Cdc42-deficient iTreg cells become unstable. The instability, but not the defective differentiation, of Cdc42-deficient iTreg cells is attributed to decreased glycolysis, suggesting that Cdc42-promoted glycolysis is important for iTreg stability but not differentiation. As Cdc42-deficient iTreg cells show decreased Hif1α, we envision that Cdc42 promotes glycolysis and its regulated iTreg stability through inducing Hif1α expression.

It remains unknown why the effects of Cdc42 deficiency are opposite between Th17 cells and iTreg cells. Of note, strong TCR signaling has been shown to promote Th17 cell differentiation but suppress iTreg cell differentiation (46–48). In this context, the enhanced Th17 differentiation and the diminished iTreg differentiation upon Cdc42 deletion may be attributed to heightened TCR signaling. Indeed, we have previously shown that Cdc42 deficiency leads to sustained ERK activation in activated T cells (23). Interestingly, Cdc42 deficiency also augments mTOR signaling in both Th17 and iTreg cells (data not shown). As mTOR is known to promote Th17 differentiation but suppress iTreg differentiation (49), the increased mTOR signaling may contribute to the agonistic effect of Cdc42 deficiency on Th17 differentiation and to the antagonistic effect of Cdc42 deficiency on iTreg differentiation. Moreover, given that mTOR is an essential metabolic sensor and is important for glycolysis in Th17 cells (27), the increased mTOR signaling may also contribute to the upregulated glycolytic signaling in Cdc42-deficient Th17 cells and to the downregulated glycolytic signaling in Cdc42-deficient iTreg cells. In addition to TCR signaling strength, the different skewing cytokines (IL-6 + TGF-β versus IL-2 + TGF-β) that drive Th17 versus iTreg differentiation may contribute to the opposite effects of Cdc42 deletion on Th17 versus iTreg cells. We speculate that on the one hand, IL-6 + TGF-β induce Th17 cell differentiation through upregulation of glycolysis, on the other hand, they activate Cdc42 to restrain glycolysis in a negative feedback manner to prevent aberrant/pathogenic Th17 cell differentiation. In iTreg cells, IL-2 + TGF-β activate Cdc42 to promote iTreg differentiation independent of glycolysis and to stabilize differentiated iTreg cells via upregulation of glycolysis.

Treg-specific deletion of Cdc42 by $Foxp3^{YFP\text{-}Cre}$ causes early, fatal inflammatory disorders, suggesting that Cdc42 is a bona fide gatekeeper of peripheral tolerance. We have found that the inflammatory disorders in $Cdc42^{fl/fl}Foxp3^{YFP\text{-}Cre}$ mice are caused by increased effector T cells and decreased nTreg cells. The decrease in nTreg cells is due to impaired proliferation, survival and stability but not differentiation. The instability of $Cdc42^{fl/fl}Foxp3^{YFP\text{-}Cre}$ nTreg cells is evidenced by downregulation of Foxp3 and upregulation of transcription factors and cytokines characteristic of effector T cells. As

reduced Foxp3 expression is known to convert Treg cells to effector T cells (40), at least a proportion of the increased effector T cells in $Cdc42^{fl/fl}Foxp3^{YFP\text{-}Cre}$ mice could have been derived from $Cdc42^{fl/fl}Foxp3^{YFP\text{-}Cre}$ nTreg cells. In support, we show that $Cdc42^{fl/fl}Foxp3^{YFP\text{-}Cre}$ nTreg cells are more susceptible to transdifferentiate to Th17 and Th1 cells in vitro, compared to $Cdc42^{+/+}Foxp3^{YFP\text{-}Cre}$ nTreg cells. Meanwhile, the appearance of $Cdc42^{fl/fl}Foxp3^{YFP\text{-}Cre}$ nTreg cells expressing effector T cell markers might have exacerbated effector T cell functions and thus lymphoproliferative diseases in $Cdc42^{fl/fl}Foxp3^{YFP\text{-}Cre}$ mice, given that Treg cells expressing effector T cell markers are implicated in autoimmune diseases such as inflammatory bowel diseases (4).

We provide evidences to indicate that the instability of $Cdc42^{fl/fl}Foxp3^{YFP\text{-}Cre}$ nTreg cells could have resulted from their activation, the Foxp3 enhancer hyper-methylation, and/or attenuated glycolysis. However, although $Cdc42^{fl/fl}Foxp3^{YFP\text{-}Cre}$ nTreg cells upregulate their activation/functional markers in a cell intrinsic manner, the activation phenotype of these cells might just reflect a compensatory effect due to the reduced frequency. On the other hand, by pyruvate rescuing, we show that the decreased glycolytic activity contributes to the instability of $Cdc42^{fl/fl}Foxp3^{YFP\text{-}Cre}$ nTreg cells, similar to that observed in Cdc42-deficient iTreg cells. Thus, our data depict that weakened glycolysis can lead to Treg instability. This is in contrast to a couple of recent studies that have associated heightened glycolysis to Treg instability (11, 12, 50). We reason that physiologic level of glycolysis is important for maintaining Treg stability. As deletion of Cdc42 links weakened glycolysis to Treg instability and deletion of PTEN or ATG7 links heightened glycolysis to Treg instability (11, 12, 50), we postulate that Cdc42 upregulates glycolysis to promote Treg stability, whereas PTEN/ATG7 controls magnitude of Cdc42-induced glycolysis to prevent hyperglycolysis-induced Treg cell destabilization.

In summary, we have identified Cdc42 as a master regulator of the balance between Th17 and iTreg or nTreg cells. Cdc42 controls Th17/iTreg balance by inhibiting aberrant differentiation/pathogenicity of Th17 cells and promoting differentiation/stability/suppressive function of iTreg cells. Cdc42 controls Th17/nTreg balance by maintaining nTreg cell homeostasis through regulating nTreg cell proliferation/survival/stability. Cdc42 may do so by integrating transcriptional and metabolic signaling in Th17 and Treg cells. Consequently, T cell-specific deletion of Cdc42 leads to exacerbated wasting disease in mouse models of colitis and Treg cell-specific deletion of Cdc42 causes spontaneous, early fatal lymphoproliferative diseases. Therefore, interference of Cd42 pathway in T cells might open a new avenue in autoimmune disease therapy and in cancer immunotherapy. Particularly, the observation that inhibition of glycolysis in Cdc42-deficient Th17 cells diminished their pathogenicity but not WT level of differentiation suggests that targeting Cdc42-regulated glycolysis selectively inhibits pathogenic but not protective Th17 cells and therefore could have important implications in the clinical therapy of Th17-mediated immune diseases.

Supplementary Material

Refer to Web version on PubMed Central for supplementary material.

Acknowledgments

This work was supported in part by grants from the National Institutes of Health (R01GM108661 and R21CA198358 to F.G.), National Natural Science Foundation of China (81373116 to J. Q.Y) and Jiangsu Provincial Project of Invigorating Health Care through Science, Technology and Education, China (to J.Q.Y).

We thank Veda Yadagiri and Hong Ji at the Cincinnati Children's Hospital Research Foundation Pyrosequencing Core for analysis of methylation of Foxp3 gene and for writing the related methods.

The authors have no financial conflict of interests.

ABBREVIATIONS

2-DG	2-Deoxy-D-glucose
CTLA-4	Cytotoxic T-lymphocyte-associated protein 4
DSS	Dextran Sulphate Sodium
DUSP2	Dual Specificity Phosphatase 2
FASN	Fatty Acid Synthase
GITR	Glucocorticoid-induced TNFR-related protein
Hif1α	Hypoxia Inducible Factor 1α
HMGCR	(3-Hydroxy-3-Methylglutaryl-CoA Reductase)
IBD	Inflammatory Bowel Disease
PD-1	Programmed cell death protein 1
PDK1	Phosphoinositide-dependent kinase-1
PGM1	Phosphoglucomutase 1
PUSA	Polyunsaturated fatty acid

References

1. Bedoya SK, Lam B, Lau K, Larkin J 3rd. Th17 cells in immunity and autoimmunity. Clin Dev Immunol. 2013; 2013:986789. [PubMed: 24454481]
2. Wang C, Yosef N, Gaublomme J, Wu C, Lee Y, Clish CB, Kaminski J, Xiao S, Meyer Zu Horste G, Pawlak M, Kishi Y, Joller N, Karwacz K, Zhu C, Ordovas-Montanes M, Madi A, Wortman I, Miyazaki T, Sobel RA, Park H, Regev A, Kuchroo VK. CD5L/AIM Regulates Lipid Biosynthesis and Restrains Th17 Cell Pathogenicity. Cell. 2015; 163:1413–1427. [PubMed: 26607793]
3. Lee Y, Awasthi A, Yosef N, Quintana FJ, Xiao S, Peters A, Wu C, Kleinewietfeld M, Kunder S, Hafler DA, Sobel RA, Regev A, Kuchroo VK. Induction and molecular signature of pathogenic TH17 cells. Nature immunology. 2012; 13:991–999. [PubMed: 22961052]
4. Ueno A, Ghosh A, Hung D, Li J, Jijon H. Th17 plasticity and its changes associated with inflammatory bowel disease. World J Gastroenterol. 2015; 21:12283–12295. [PubMed: 26604637]
5. Ohkura N, Kitagawa Y, Sakaguchi S. Development and maintenance of regulatory T cells. Immunity. 2013; 38:414–423. [PubMed: 23521883]

6. Dang EV, Barbi J, Yang HY, Jinasena D, Yu H, Zheng Y, Bordman Z, Fu J, Kim Y, Yen HR, Luo W, Zeller K, Shimoda L, Topalian SL, Semenza GL, Dang CV, Pardoll DM, Pan F. Control of T(H)17/T(reg) balance by hypoxia-inducible factor 1. Cell. 2011; 146:772–784. [PubMed: 21871655]
7. Gomez-Rodriguez J, Wohlfert EA, Handon R, Meylan F, Wu JZ, Anderson SM, Kirby MR, Belkaid Y, Schwartzberg PL. Itk-mediated integration of T cell receptor and cytokine signaling regulates the balance between Th17 and regulatory T cells. The Journal of experimental medicine. 2014; 211:529–543. [PubMed: 24534190]
8. Basu R, Whitley SK, Bhaumik S, Zindl CL, Schoeb TR, Benveniste EN, Pear WS, Hatton RD, Weaver CT. IL-1 signaling modulates activation of STAT transcription factors to antagonize retinoic acid signaling and control the TH17 cell-iTreg cell balance. Nature immunology. 2015; 16:286–295. [PubMed: 25642823]
9. Barbi J, Pardoll DM, Pan F. Ubiquitin-dependent regulation of Foxp3 and Treg function. Immunol Rev. 2015; 266:27–45. [PubMed: 26085205]
10. Takahashi R, Nishimoto S, Muto G, Sekiya T, Tamiya T, Kimura A, Morita R, Asakawa M, Chinen T, Yoshimura A. SOCS1 is essential for regulatory T cell functions by preventing loss of Foxp3 expression as well as IFN-{gamma} and IL-17A production. The Journal of experimental medicine. 2011; 208:2055–2067. [PubMed: 21893603]
11. Shrestha S, Yang K, Guy C, Vogel P, Neale G, Chi H. Treg cells require the phosphatase PTEN to restrain TH1 and TFH cell responses. Nature immunology. 2015; 16:178–187. [PubMed: 25559258]
12. Huynh A, DuPage M, Priyadharshini B, Sage PT, Quiros J, Borges CM, Townamchai N, Gerriets VA, Rathmell JC, Sharpe AH, Bluestone JA, Turka LA. Control of PI(3) kinase in Treg cells maintains homeostasis and lineage stability. Nature immunology. 2015; 16:188–196. [PubMed: 25559257]
13. Yang XO, Nurieva R, Martinez GJ, Kang HS, Chung Y, Pappu BP, Shah B, Chang SH, Schluns KS, Watowich SS, Feng XH, Jetten AM, Dong C. Molecular antagonism and plasticity of regulatory and inflammatory T cell programs. Immunity. 2008; 29:44–56. [PubMed: 18585065]
14. Sekiya T, Kondo T, Shichita T, Morita R, Ichinose H, Yoshimura A. Suppression of Th2 and Tfh immune reactions by Nr4a receptors in mature T reg cells. The Journal of experimental medicine. 2015; 212:1623–1640. [PubMed: 26304965]
15. Sebastian M, Lopez-Ocasio M, Metidji A, Rieder SA, Shevach EM, Thornton AM. Helios Controls a Limited Subset of Regulatory T Cell Functions. Journal of immunology. 2016; 196:144–155.
16. Nakagawa H, Sido JM, Reyes EE, Kiers V, Cantor H, Kim HJ. Instability of Helios-deficient Tregs is associated with conversion to a T-effector phenotype and enhanced antitumor immunity. Proc Natl Acad Sci U S A. 2016; 113:6248–6253. [PubMed: 27185917]
17. Melendez J, Grogg M, Zheng Y. Signaling role of Cdc42 in regulating mammalian physiology. The Journal of biological chemistry. 2011; 286:2375–2381. [PubMed: 21115489]
18. Etienne-Manneville S, Hall A. Rho GTPases in cell biology. Nature. 2002; 420:629–635. [PubMed: 12478284]
19. Stowers L, Yelon D, Berg LJ, Chant J. Regulation of the polarization of T cells toward antigen-presenting cells by Ras-related GTPase CDC42. Proc Natl Acad Sci U S A. 1995; 92:5027–5031. [PubMed: 7761442]
20. Tskvitaria-Fuller I, Seth A, Mistry N, Gu H, Rosen MK, Wulfing C. Specific patterns of Cdc42 activity are related to distinct elements of T cell polarization. Journal of immunology. 2006; 177:1708–1720.
21. Haddad E, Zugaza JL, Louache F, Debili N, Crouin C, Schwarz K, Fischer A, Vainchenker W, Bertoglio J. The interaction between Cdc42 and WASP is required for SDF-1-induced T-lymphocyte chemotaxis. Blood. 2001; 97:33–38. [PubMed: 11133739]
22. Na S, Li B, Grewal IS, Enslen H, Davis RJ, Hanke JH, Flavell RA. Expression of activated CDC42 induces T cell apoptosis in thymus and peripheral lymph organs via different pathways. Oncogene. 1999; 18:7966–7974. [PubMed: 10637507]
23. Guo F, Hildeman D, Tripathi P, Velu CS, Grimes HL, Zheng Y. Coordination of IL-7 receptor and T-cell receptor signaling by cell-division cycle 42 in T-cell homeostasis. Proc Natl Acad Sci U S A. 2010; 107:18505–18510. [PubMed: 20937872]

24. Guo F, Zhang S, Tripathi P, Mattner J, Phelan J, Sproles A, Mo J, Wills-Karp M, Grimes HL, Hildeman D, Zheng Y. Distinct roles of Cdc42 in thymopoiesis and effector and memory T cell differentiation. PLoS One. 2011; 6:e18002. [PubMed: 21455314]
25. Yang L, Wang L, Kalfa TA, Cancelas JA, Shang X, Pushkaran S, Mo J, Williams DA, Zheng Y. Cdc42 critically regulates the balance between myelopoiesis and erythropoiesis. Blood. 2007; 110:3853–3861. [PubMed: 17702896]
26. Lu D, Liu L, Ji X, Gao Y, Chen X, Liu Y, Liu Y, Zhao X, Li Y, Li Y, Jin Y, Zhang Y, McNutt MA, Yin Y. The phosphatase DUSP2 controls the activity of the transcription activator STAT3 and regulates TH17 differentiation. Nature immunology. 2015; 16:1263–1273. [PubMed: 26479789]
27. Shi LZ, Wang R, Huang G, Vogel P, Neale G, Green DR, Chi H. HIF1alpha-dependent glycolytic pathway orchestrates a metabolic checkpoint for the differentiation of TH17 and Treg cells. The Journal of experimental medicine. 2011; 208:1367–1376. [PubMed: 21708926]
28. Berod L, Friedrich C, Nandan A, Freitag J, Hagemann S, Harmrolfs K, Sandouk A, Hesse C, Castro CN, Bahre H, Tschirner SK, Gorinski N, Gohmert M, Mayer CT, Huehn J, Ponimaskin E, Abraham WR, Muller R, Lochner M, Sparwasser T. De novo fatty acid synthesis controls the fate between regulatory T and T helper 17 cells. Nature medicine. 2014; 20:1327–1333.
29. Harbour SN, Maynard CL, Zindl CL, Schoeb TR, Weaver CT. Th17 cells give rise to Th1 cells that are required for the pathogenesis of colitis. Proc Natl Acad Sci U S A. 2015; 112:7061–7066. [PubMed: 26038559]
30. Kiesler P I, Fuss J, Strober W. Experimental Models of Inflammatory Bowel Diseases. Cell Mol Gastroenterol Hepatol. 2015; 1:154–170. [PubMed: 26000334]
31. Michalek RD V, Gerriets A, Jacobs SR, Macintyre AN, MacIver NJ, Mason EF, Sullivan SA, Nichols AG, Rathmell JC. Cutting edge: distinct glycolytic and lipid oxidative metabolic programs are essential for effector and regulatory CD4+ T cell subsets. Journal of immunology. 2011; 186:3299–3303.
32. Newton R, Priyadharshini B, Turka LA. Immunometabolism of regulatory T cells. Nature immunology. 2016; 17:618–625. [PubMed: 27196520]
33. Gerriets VA, Kishton RJ, Johnson MO, Cohen S, Siska PJ, Nichols AG, Warmoes MO, de Cubas AA, MacIver NJ, Locasale JW, Turka LA, Wells AD, Rathmell JC. Foxp3 and Toll-like receptor signaling balance Treg cell anabolic metabolism for suppression. Nature immunology. 2016; 17:1459–1466. [PubMed: 27695003]
34. Gerriets VA, Kishton RJ, Nichols AG, Macintyre AN, Inoue M, Ilkayeva O, Winter PS, Liu X, Priyadharshini B, Slawinska ME, Haeberli L, Huck C, Turka LA, Wood KC, Hale LP, Smith PA, Schneider MA, MacIver NJ, Locasale JW, Newgard CB, Shinohara ML, Rathmell JC. Metabolic programming and PDHK1 control CD4+ T cell subsets and inflammation. The Journal of clinical investigation. 2015; 125:194–207. [PubMed: 25437876]
35. Andrabi SA, Umanah GK, Chang C, Stevens DA, Karuppagounder SS, Gagne JP, Poirier GG, Dawson VL, Dawson TM. Poly(ADP-ribose) polymerase-dependent energy depletion occurs through inhibition of glycolysis. Proc Natl Acad Sci U S A. 2014; 111:10209–10214. [PubMed: 24987120]
36. Hadaschik EN, Wei X, Leiss H, Heckmann B, Niederreiter B, Steiner G, Ulrich W, Enk AH, Smolen JS, Stummvoll GH. Regulatory T cell-deficient scurfy mice develop systemic autoimmune features resembling lupus-like disease. Arthritis Res Ther. 2015; 17:35. [PubMed: 25890083]
37. Lahl K, Loddenkemper C, Drouin C, Freyer J, Arnason J, Eberl G, Hamann A, Wagner H, Huehn J, Sparwasser T. Selective depletion of Foxp3+ regulatory T cells induces a scurfy-like disease. The Journal of experimental medicine. 2007; 204:57–63. [PubMed: 17200412]
38. Kim JM, Rasmussen JP, Rudensky AY. Regulatory T cells prevent catastrophic autoimmunity throughout the lifespan of mice. Nature immunology. 2007; 8:191–197. [PubMed: 17136045]
39. Feng Y, Arvey A, Chinen T, van der Veeken J, Gasteiger G, Rudensky AY. Control of the inheritance of regulatory T cell identity by a cis element in the Foxp3 locus. Cell. 2014; 158:749–763. [PubMed: 25126783]
40. Wan YY, Flavell RA. Regulatory T-cell functions are subverted and converted owing to attenuated Foxp3 expression. Nature. 2007; 445:766–770. [PubMed: 17220876]

41. Zhang Z, Zhang W, Guo J, Gu Q, Zhu X, Zhou X. Activation and Functional Specialization of Regulatory T Cells Lead to the Generation of Foxp3 Instability. Journal of immunology. 2017; 198:2612–2625.
42. Zheng Y, Josefowicz S, Chaudhry A, Peng XP, Forbush K, Rudensky AY. Role of conserved non-coding DNA elements in the Foxp3 gene in regulatory T-cell fate. Nature. 2010; 463:808–812. [PubMed: 20072126]
43. Bailey-Bucktrout SL, Martinez-Llordella M, Zhou X, Anthony B, Rosenthal W, Luche H, Fehling HJ, Bluestone JA. Self-antigen-driven activation induces instability of regulatory T cells during an inflammatory autoimmune response. Immunity. 2013; 39:949–962. [PubMed: 24238343]
44. Komatsu N, Okamoto K, Sawa S, Nakashima T, Oh-hora M, Kodama T, Tanaka S, Bluestone JA, Takayanagi H. Pathogenic conversion of Foxp3+ T cells into TH17 cells in autoimmune arthritis. Nature medicine. 2014; 20:62–68.
45. Zhou X, Bailey-Bucktrout SL, Jeker LT, Penaranda C, Martinez-Llordella M, Ashby M, Nakayama M, Rosenthal W, Bluestone JA. Instability of the transcription factor Foxp3 leads to the generation of pathogenic memory T cells in vivo. Nature immunology. 2009; 10:1000–1007. [PubMed: 19633673]
46. Li C, Ebert PJ, Li QJ. T Cell Receptor (TCR) and Transforming Growth Factor β (TGF-β) Signaling Converge on DNA (Cytosine-5)-methyltransferase to Control *forkhead box protein 3* (*foxp3*) Locus Methylation and Inducible Regulatory T Cell Differentiation. Journnal of Biological Chemistry. 2013; 288:19127–19139.
47. van Panhuys N. TCR Signal Strength Alters T-DC Activation and Interaction Times and Directs the Outcome of Differentiation. Frontiers in Immunology. 2016; 7:6. [PubMed: 26834747]
48. Iezzi G, Sonderegger I, Ampenberger F, Schmitz N, Marsland BJ, Kopf M. CD40-CD40L cross-talk integrates strong antigenic signals and microbial stimuli to induce development of IL-17-producing CD4+ T cells. Proceedings of the National Academy of Sciences of the United States of America. 2009; 106:876–881. [PubMed: 19136631]
49. Delgoffe GM, Kole TP, Zheng Y, Zarek PE, Matthews KL, Xiao B, Worley PF, Kozma SC, Powell JD. The mTOR kinase differentially regulates effector and regulatory T cell lineage commitment. Immunity. 2009; 30(6):832–844. [PubMed: 19538929]
50. Wei J, Long L, Yang K, Guy C, Shrestha S, Chen Z, Wu C, Vogel P, Neale G, Green DR, Chi H. Autophagy enforces functional integrity of regulatory T cells by coupling environmental cues and metabolic homeostasis. Nature immunology. 2016; 17:277–285. [PubMed: 26808230]

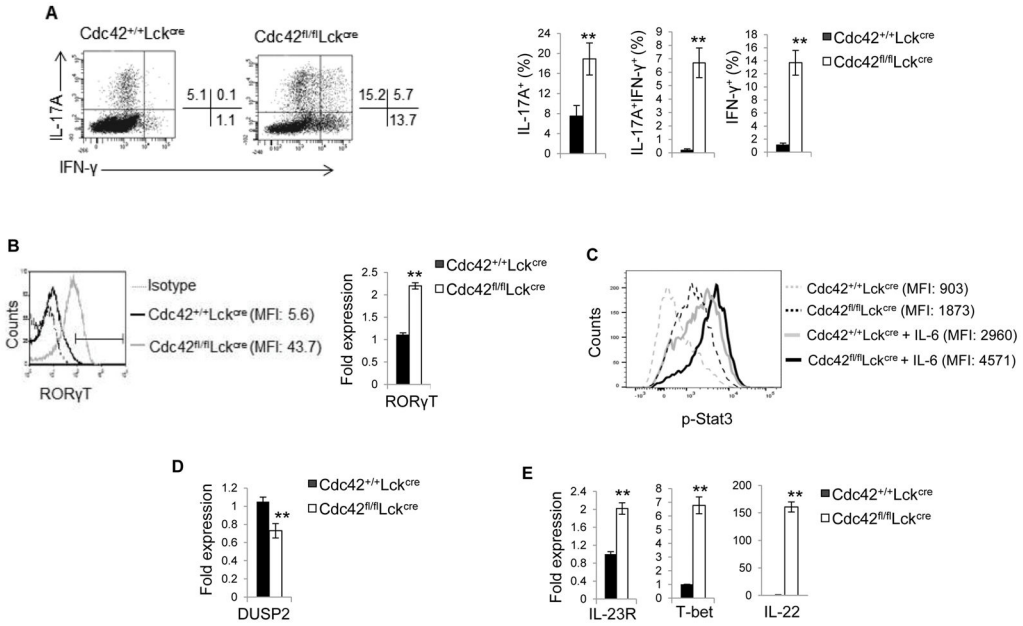

Figure 1.

Cdc42 deficiency enhances Th17 differentiation and converts non-pathogenic Th17 cells to pathogenic Th17 Cells. (**A**) Representative flow cytogram of $CD4^+$ T cells from $Cdc42^{+/+}Lck^{Cre}$ and $Cdc42^{fl/fl}Lck^{Cre}$ mice cultured under Th17 polarizing condition and stained for IL-17 and IFN-γ. Numbers besides dot plots indicate percentages of IL-17^+, $IL17^+IFN\gamma^+$ and IFN-γ^+ cells in corresponding quadrant (left). Average percentages of IL-17^+, $IL17^+IFN\gamma^+$ and IFN-γ^+ cells are shown in bar graph (right). (**B**) Mean fluorescence intensity (MFI) (left) and mRNA expression (right) of RORγT in $Cdc42^{+/+}Lck^{Cre}$ and $Cdc42^{fl/fl}Lck^{Cre}$ $CD4^+$ T cells cultured under Th17 polarizing condition. (**C**) MFI of phospho (p)-Stat3 in $Cdc42^{+/+}Lck^{Cre}$ and $Cdc42^{fl/fl}Lck^{Cre}$ $CD4^+$ T cells cultured under Th17 polarizing condition and restimulated with or without IL-6. (**D**) mRNA expression of DUSP2 in $Cdc42^{+/+}Lck^{Cre}$ and $Cdc42^{fl/fl}Lck^{Cre}$ naïve $CD4^+$ T cells cultured under Th17 polarizing condition. (**E**) mRNA expression of Th17 pathogenic genes in $Cdc42^{+/+}Lck^{Cre}$ and $Cdc42^{fl/fl}Lck^{Cre}$ naïve $CD4^+$ T cells cultured under Th17 polarizing condition. $n \geq 5$. Data are representative of three independent experiments. Error bars indicate SD. $^{**}p < 0.01$.

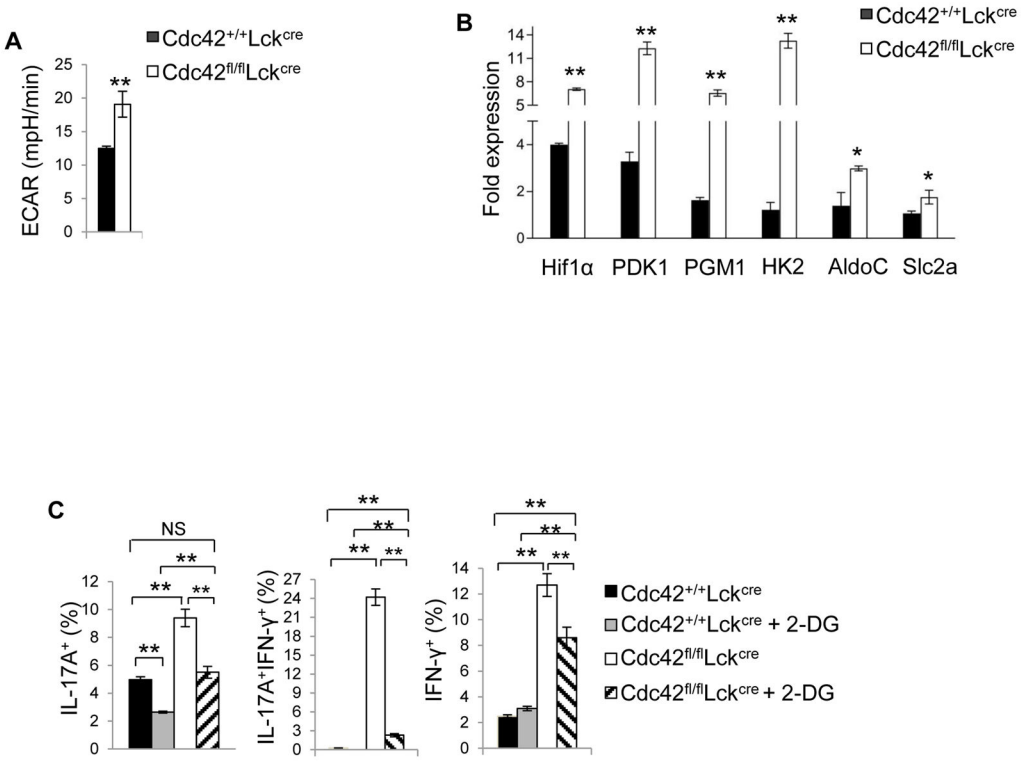

Figure 2.

Cdc42 suppresses aberrant Th17 differentiation and Th17 pathogenicity through repression of glycolysis. (**A**) ECAR of $Cdc42^{+/+}Lck^{Cre}$ and $Cdc42^{fl/fl}Lck^{Cre}$ naïve $CD4^+$ T cells cultured for 4 days under Th17 polarizing condition. (**B**) Real-time RT-PCR analysis of mRNA expression of glycolytic genes in $Cdc42^{+/+}Lck^{Cre}$ and $Cdc42^{fl/fl}Lck^{Cre}$ naïve $CD4^+$ T cells cultured under Th17 polarizing condition. (**C**) Percentages of $IL\text{-}17^+$, $IL17^+IFN\gamma^+$ and $IFN\text{-}\gamma^+$ cells derived from $Cdc42^{+/+}Lck^{Cre}$ and $Cdc42^{fl/fl}Lck^{Cre}$ naïve $CD4^+$ T cells cultured under Th17 polarizing condition in the presence or absence of 0.3 mM 2-DG. $n \geq 5$. Error bars indicate SD. $^*p < 0.05$, $^{**}p < 0.01$.

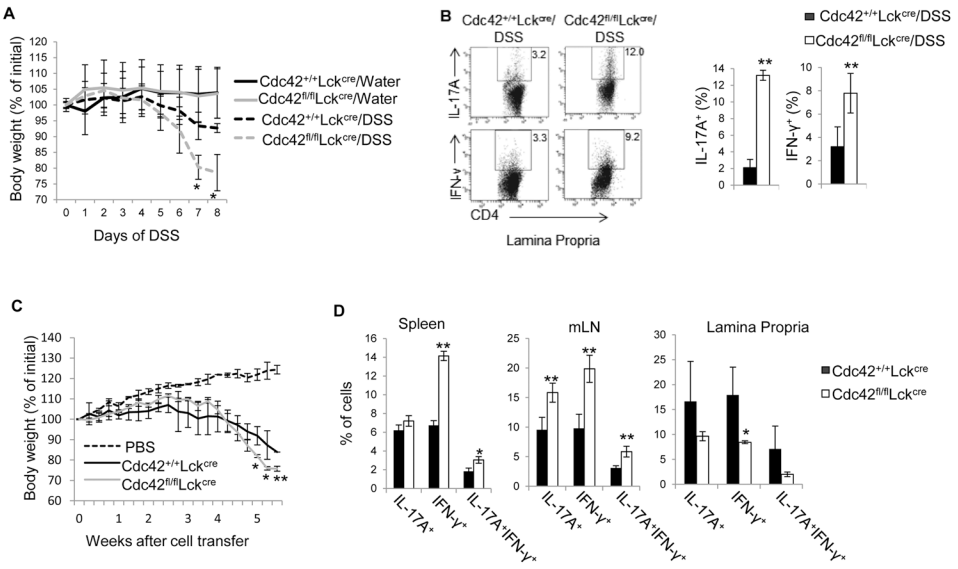

Figure 3.

Cdc42 deficiency increases disease severity of colitis. (**A**) Body weight loss of $Cdc42^{+/+}Lck^{Cre}$ and $Cdc42^{fl/fl}Lck^{Cre}$ mice treated with DSS in drinking water or normal water only. The data are expressed as percentage of initial body weight. (**B**) Representative flow cytogram of IL-17- and IFN-γ-producing $CD4^+$ cells in the lamina propria of DSS-treated $Cdc42^{+/+}Lck^{Cre}$ and $Cdc42^{fl/fl}Lck^{Cre}$ mice. Numbers in dot plots indicate percentages of IL-17- and IFN-γ-producing $CD4^+$ cells (left). Average percentages of IL-17- and IFN-γ-producing $CD4^+$ cells are shown in bar graph (right). (**C**) Body weight loss of $RAG1^{-/-}$ mice transferred with naïve $CD4^+$ T cells from $Cdc42^{+/+}Lck^{Cre}$ and $Cdc42^{fl/fl}Lck^{Cre}$ mice. (**D**) Average percentages of $IL\text{-}17^+$, IFN-γ^+ and $IL\text{-}17^+IFN\gamma^+$ cells in the spleen, mLN and lamina propria of $RAG1^{-/-}$ mice in (C). n = 5. Error bars indicate SD. *p < 0.05, **p < 0.01.

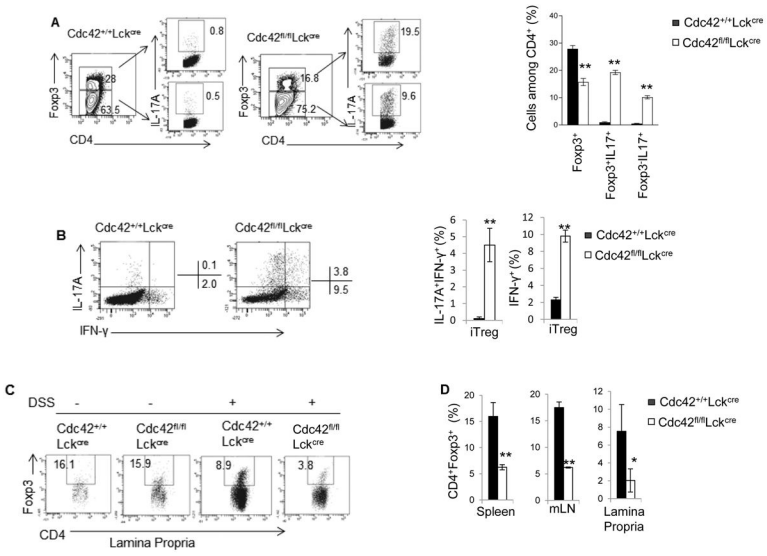

Figure 4.

Cdc42 deficiency leads to an impaired iTreg differentiation and stability in vitro and in vivo. (**A**) Representative flow cytogram of $CD4^+$ T cells from $Cdc42^{+/+}Lck^{Cre}$ and $Cdc42^{fl/fl}Lck^{Cre}$ mice cultured under iTreg polarizing condition and stained for IL-17 and Foxp3. Numbers in dot plots indicate percentages of $Foxp3^+$, $Foxp3^+IL\text{-}17^+$ and $Foxp^-IL\text{-}17^+$ cells (left). Average percentages of $Foxp3^+$, $Foxp3^+IL\text{-}17^+$ and $Foxp^-IL\text{-}17^+$ cells are shown in bar graph (right). (**B**) Representative flow cytogram of cells from (A) stained for IL-17 and IFN-γ. Numbers besides dot plots indicate percentages of $IL\text{-}17^+IFN\text{-}\gamma^+$ and $IFN\text{-}\gamma^+$ cells in corresponding quadrant (left). Average percentages of $IL\text{-}17^+IFN\text{-}\gamma^+$ and $IFN\text{-}\gamma^+$ cells are shown in bar graph (right). (**C**) Representative flow cytogram of $CD4^+Foxp3^+$ cells in the lamina propria of $Cdc42^{+/+}Lck^{Cre}$ and $Cdc42^{fl/fl}Lck^{Cre}$ mice treated with or without DSS. Numbers indicate percentages of $CD4^+Foxp3^+$ cells. (**D**) Average percentages of $CD4^+Foxp3^+$ cells in the spleen, mLN and lamina propria of $RAG1^{-/-}$ mice transferred with naïve $CD4^+$ T cells from $Cdc42^{+/+}Lck^{Cre}$ or $Cdc42^{fl/fl}Lck^{Cre}$ mice. $n \geq 5$. Data are representative of three independent experiments. Error bars indicate SD. $^*p < 0.05$, $^{**}p < 0.01$.

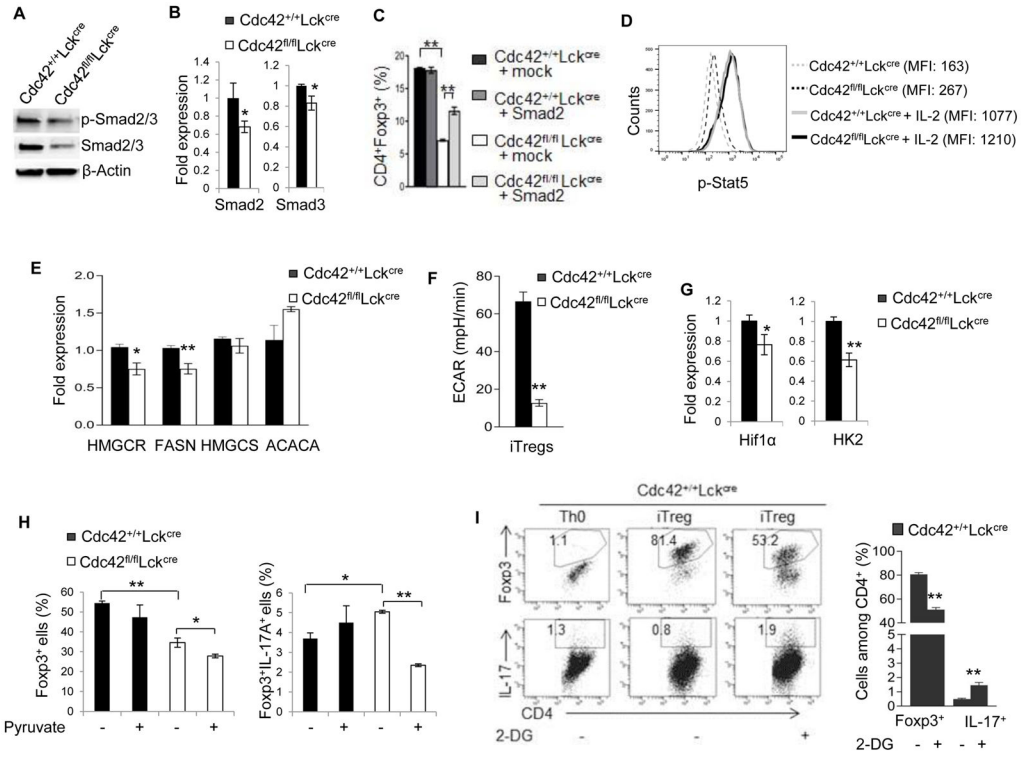

Figure 5.

Cdc42 deficiency in iTreg inhibits transcriptional and metabolic signaling and restoration of glycolysis rescues instability but not differentiation of Cdc42-deficient iTreg. (**A**) Immunoblotting of p-Smad2/3 and total Smad2/3 in $Cdc42^{+/+}Lck^{Cre}$ and $Cdc42^{fl/fl}Lck^{Cre}$ iTreg. (**B**) Real-time RT-PCR analysis of Smad2 and Smad3 mRNA expression in $Cdc42^{+/+}Lck^{Cre}$ and $Cdc42^{fl/fl}Lck^{Cre}$ iTreg. (**C**) Average percentages of $CD4^{+}Foxp3^{+}$ cells from naïve T cells that were activated, transduced with retroviral mock vector or Smad2, cultured under iTreg polarizing condition, and then stained for CD4 and Foxp3 and analyzed by FACS. (**D**) Expression (mean fluorescence intensity, MFI) of p-Stat5 in $Cdc42^{+/+}Lck^{Cre}$ and $Cdc42^{fl/fl}Lck^{Cre}$ iTreg re-stimulated with or without IL-2 for 2 h. (**E**) Real-time RT-PCR analysis of mRNA expression of lipid metabolism genes in $Cdc42^{+/+}Lck^{Cre}$ and $Cdc42^{fl/fl}Lck^{Cre}$ iTreg. (**F**) ECAR of $Cdc42^{+/+}Lck^{Cre}$ and $Cdc42^{fl/fl}Lck^{Cre}$ iTreg. (**G**) Real-time RT-PCR analysis of mRNA expression of glycolytic genes in $Cdc42^{+/+}Lck^{Cre}$ and $Cdc42^{fl/fl}Lck^{Cre}$ iTreg. (**H**) Percentages of $Foxp3^{+}$ and $Foxp3^{+}IL17^{+}$ cells derived from $Cdc42^{+/+}Lck^{Cre}$ and $Cdc42^{fl/fl}Lck^{Cre}$ naïve $CD4^{+}$ T cells cultured under iTreg polarizing condition in the presence or absence of 2 mM pyruvate. (**I**) Representative flow cytogram of $CD4^{+}$ naïve T cells from $Cdc42^{+/+}Lck^{Cre}$ mice cultured under Th0 or iTreg polarizing condition in the presence or absence of 0.3 mM 2-DG and stained for Foxp3 and IL-17. Numbers in dot plots indicate percentages of $Foxp3^{+}$ and IL-17^{+} cells (left). Average percentages of $Foxp3^{+}$ and IL-17^{+} cells are shown in bar graph (right). n = 5. Error bars indicate SD. *p < 0.05, **p < 0.01.

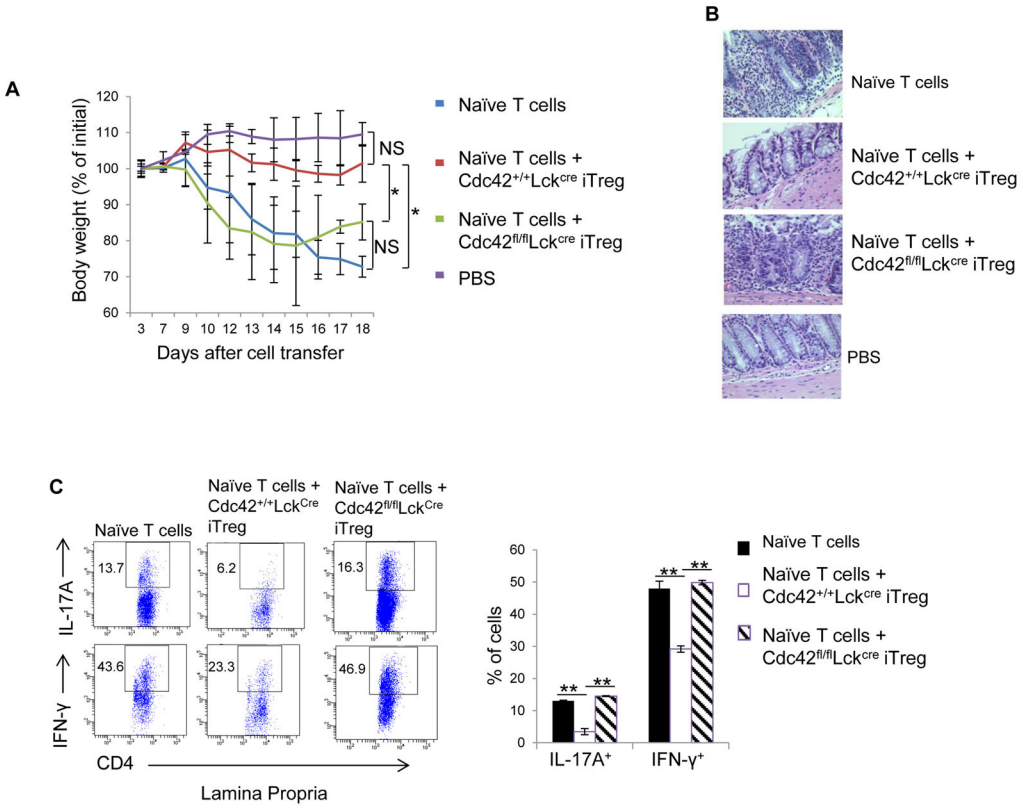

Figure 6.

Cdc42 deficiency inhibits iTreg suppressive function. (**A**) Body weight loss of RAG1$^{-/-}$ mice transferred with naïve CD4^{+} T cells only or naïve CD4^{+} T cells in combination with Cdc42$^{+/+}$Lck^{Cre} or Cdc42$^{fl/fl}$Lck^{Cre} iTreg. (**B**) Representative images of hematoxylin and eosin staining of the lamina propria of RAG1$^{-/-}$ mice from (A). (**C**) Representative flow cytogram of IL-17- and IFN-γ-producing CD4^{+} cells in the lamina propria of RAG1$^{-/-}$ mice from (A). Numbers in dot plots indicate percentages of IL-17- and IFN-γ-producing CD4^{+} cells (left). Average percentages of IL-17- and IFN-γ-producing CD4^{+} cells are shown in bar graph (right). n = 5. Error bars indicate SD. *p < 0.05 at day 17 and day 18, **p < 0.01. NS: no significance.

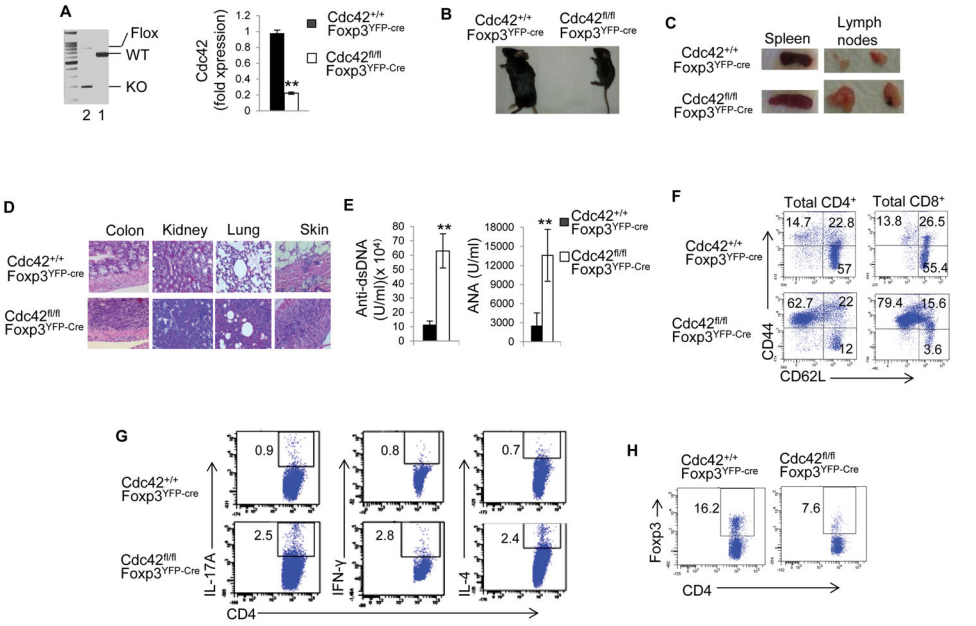

Figure 7.

Treg-specific deletion of Cdc42 causes a fatal spontaneous inflammatory disorder. (**A**) Left, Genotyping of wild type (WT), knockout (KO) and floxed (Flox) allele of Cdc42 in $CD4^+Foxp3^+YFP^+$ cells from $Cdc42^{+/+}Foxp3^{YFP\text{-}Cre}$ and $Cdc42^{fl/fl}Foxp3^{YFP\text{-}Cre}$ mice. 1, $Cdc42^{+/+}Foxp3^{YFP\text{-}Cre}$; 2, $Cdc42^{fl/fl}Foxp3^{YFP\text{-}Cre}$. Right, Real-time RT-PCR analysis of Cdc42 mRNA expression in $CD4^+Foxp3^+YFP^+$ cells. Three to four weeks old mice were used. (**B**) Representative image of $Cdc42^{+/+}Foxp3^{YFP\text{-}Cre}$ and $Cdc42^{fl/fl}$ $Foxp3^{YFP\text{-}Cre}$ mice. (**C**) Representative images of splenomegaly and lymphadenopathy in $Cdc42^{fl/fl}Foxp3^{YFP\text{-}Cre}$ mice. inguinal and axilliary lymph nodes are shown. (**D**) Representative images of hematoxylin and eosin staining of the colon, kidney, lung and skin from $Cdc42^{fl/fl}$ $Foxp3^{YFP\text{-}Cre}$ and $Cdc42^{+/+}Foxp3^{YFP\text{-}Cre}$ mice. (**E**) ELISA analysis of anti-dsDNA and anti-nuclear autoantibodies in the serum of $Cdc42^{+/+}Foxp3^{YFP\text{-}Cre}$ and $Cdc42^{fl/fl}Foxp3^{YFP\text{-}Cre}$ mice. (**F**) Representative flow cytogram of splenocytes from $Cdc42^{+/+}Foxp3^{YFP\text{-}Cre}$ and $Cdc42^{fl/fl}$ $Foxp3^{YFP\text{-}Cre}$ mice stained for CD44 and CD62L among $CD4^+$ and $CD8^+$ cells. Numbers indicate percentages of $CD44^+$, $CD44^+CD62L^+$, and $CD62L^+$ cells. (**G**) Representative flow cytogram of splenocytes from $Cdc42^{+/+}Foxp3^{YFP\text{-}Cre}$ and $Cdc42^{fl/fl}$ $Foxp3^{YFP\text{-}Cre}$ mice stained for IL-17, IFN-γ and IL-4 among $CD4^+$ cells. Numbers indicate percentages of $IL\text{-}17^+$, $IFN\text{-}\gamma^+$ and $IL\text{-}4^+$ cells. (**H**) Representative flow cytogram of splenocytes from $Cdc42^{+/+}Foxp3^{YFP\text{-}Cre}$ and $Cdc42^{fl/fl}Foxp3^{YFP\text{-}Cre}$ mice stained for Foxp3 and CD4. Numbers indicate percentages of $CD4^+Foxp3^+$ cells. n = 3. Data are representative of three independent experiments. Error bars indicate SD. $^{**}p < 0.01$.

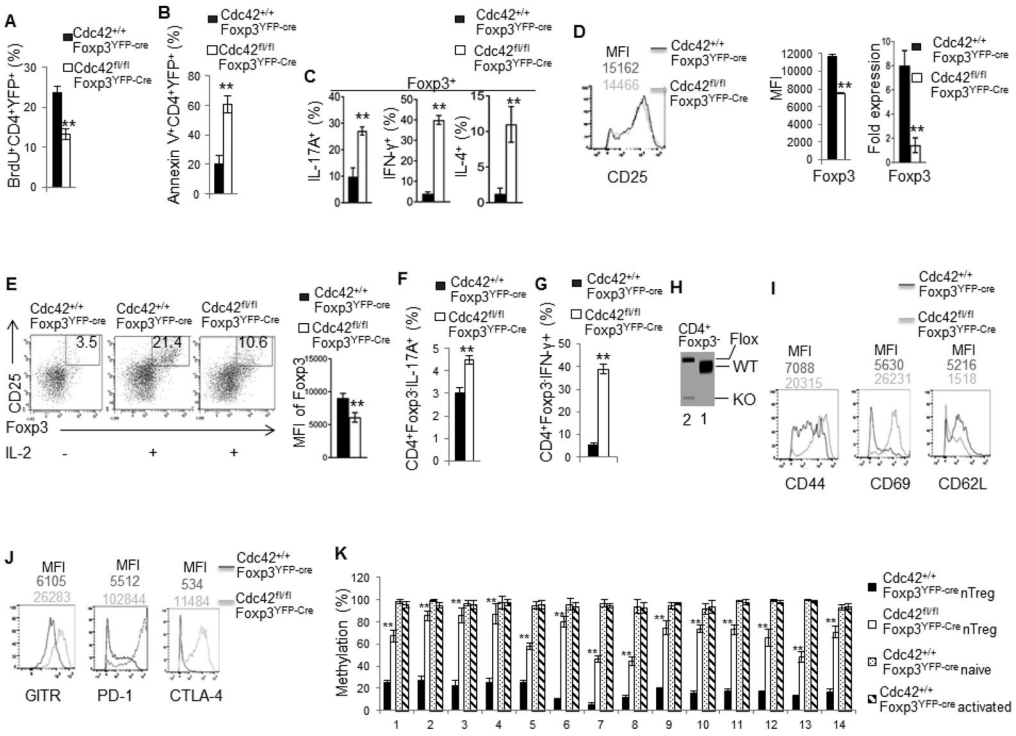

Figure 8.

Treg-specific deletion of Cdc42 leads to impaired Treg proliferation, survival and stability. (**A**) Percentages of BrdU-incorporated cells among $CD4^+YFP^+$ cells from the spleen of $Cdc42^{+/+}Foxp3^{YFP\text{-}Cre}$ and $Cdc42^{fl/fl}Foxp3^{YFP\text{-}Cre}$ mice. (**B**) Percentages of apoptotic cells (total Annexin V^+) among $CD4^+YFP^+$ cells from the spleen of $Cdc42^{+/+}Foxp3^{YFP\text{-}Cre}$ and $Cdc42^{fl/fl}Foxp3^{YFP\text{-}Cre}$ mice. (**C**) Percentages of IL-17^+, IFN-γ^+ and IL-4^+ cells among $Foxp3^+$ population in the splenocytes from $Cdc42^{+/+}Foxp3^{YFP\text{-}Cre}$ and $Cdc42^{fl/fl}Foxp3^{YFP\text{-}Cre}$ mice. (**D**) Protein expression (MFI) of CD25 (left) and Foxp3 (middle) and mRNA expression of Foxp3 (right) in $CD4^+Foxp3^+$ cells from the spleen of $Cdc42^{+/+}Foxp3^{YFP\text{-}Cre}$ and $Cdc42^{fl/fl}Foxp3^{YFP\text{-}Cre}$ mice. (**E**) $CD4^+CD25^+YFP^+$ nTreg cells were purified from $Cdc42^{+/+}Foxp3^{YFP\text{-}Cre}$ and $Cdc42^{fl/fl}Foxp3^{YFP\text{-}Cre}$ mice and cultured with anti-CD3/-CD28 and IL-2 (10 ng/ml) for 36 h and costained for Foxp3 and CD25. Left, Representative flow cytogram of Foxp3 and CD25 costaining. Numbers in the dot plots indicate percentages of $Foxp3^+CD25^+$ cells. Right, Foxp3 expression (MFI). (**F**) Purified $CD4^+CD25^+YFP^+$ nTreg cells were cultured with anti-CD3/-CD28, IL-1β (50 ng/ml) and IL-6 (40 ng/ml) for 36 h and costained for CD4, Foxp3, and IL-17. Percentages of $CD4^+Foxp3^-$IL-17^+ are shown. (**G**) Purified $CD4^+CD25^+YFP^+$ nTreg cells were cultured with anti-CD3/-CD28 and IL-12 (50 ng/ml) for 36 h and costained for CD4, Foxp3, and IFN-γ. Percentages of $CD4^+Foxp3^-$IFN-γ^+ are shown. (**H**) Genotyping of wild type (WT), knockout (KO) and floxed (Flox) allele of Cdc42 in $CD4^+Foxp3^-$ cells from the spleen of $Cdc42^{+/+}Foxp3^{YFP\text{-}Cre}$ and $Cdc42^{fl/fl}Foxp3^{YFP\text{-}Cre}$ mice. 1, $Cdc42^{+/+}Foxp3^{YFP\text{-}Cre}$; 2, $Cdc42^{fl/fl}Foxp3^{YFP\text{-}Cre}$. (**I, J**) Expression of CD44, CD69 and CD62L (I) and GITR, PD-1 and CTLA-4 (J) in $CD4^+Foxp3^+$ cells from the spleen of $Cdc42^{+/+}Foxp3^{YFP\text{-}Cre}$ and $Cdc42^{fl/fl}Foxp3^{YFP\text{-}Cre}$ mice. Numbers above the graphs indicate mean fluorescence

intensity (MFI). (**K**) Methylation status of 14 methylation sites of the Foxp3 CNS2 locus, detected by bisulfite pyrosequencing of naïve CD4+ T cells and anti-CD3/-CD28-activated $CD4^+$ T cells as controls and $CD4^+Foxp3^+YFP^+$ nTreg cells from the spleen of $Cdc42^{+/+}Foxp3^{YFP\text{-}Cre}$ and/or $Cdc42^{fl/fl}Foxp3^{YFP\text{-}Cre}$ mice. Data are expressed as percentage of methylation which indicates percent cells with a particular methylation site methylated. For (A–J), n = 5. Data are representative of three independent experiments. Error bars indicate SD. For (K), data are from one experiment with 4–5 mice pooled. Error bars indicate SD of triplicates. *$p < 0.05$, **$p < 0.01$.

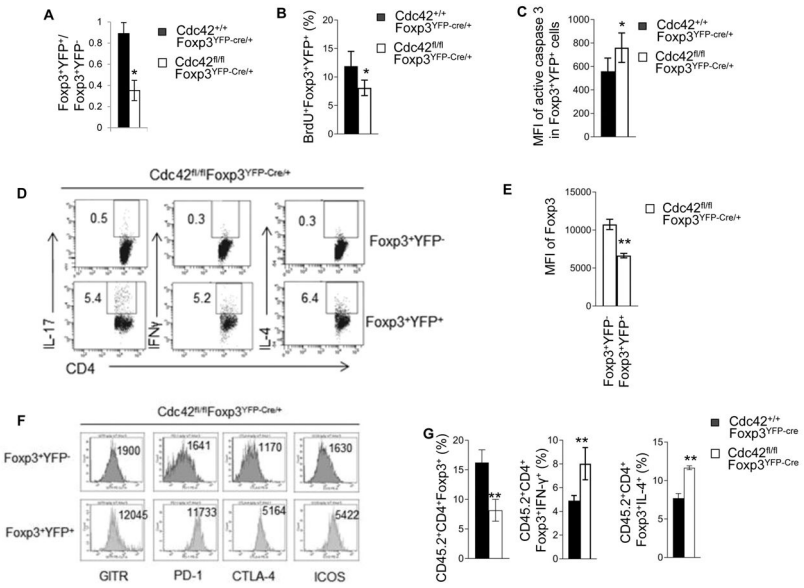

Figure 9.

Cdc42-deficient nTreg cells from $Cdc42^{fl/fl}Foxp3^{YFP\text{-}Cre/+}$ mice and from $Cdc42^{fl/fl}Foxp3^{YFP\text{-}Cre}$ bone marrow chimeric mice are impaired in competitiveness and stability. (**A**) The ratio of $Foxp3^{+}YFP^{+}$ vs $Foxp3^{+}YFP^{-}$ cells from the spleen of $Cdc42^{+/+}Foxp3^{YFP\text{-}Cre/+}$ and $Cdc42^{fl/fl}$ $Foxp3^{YFP\text{-}Cre/+}$ mice. (**B**) Percentages of BrdU-incorporated cells among $Foxp3^{+}YFP^{+}$ cells from the spleen of $Cdc42^{+/+}Foxp3^{YFP\text{-}Cre/+}$ and $Cdc42^{fl/fl}Foxp3^{YFP\text{-}Cre/+}$ mice. (**C**) Mean fluorescence intensity (MFI) of active caspase 3 among $Foxp3^{+}YFP^{+}$ cells from the spleen of $Cdc42^{+/+}Foxp3^{YFP\text{-}Cre/+}$ and $Cdc42^{fl/fl}Foxp3^{YFP\text{-}Cre/+}$ mice. (**D**) Representative flow cytogram of staining of IL-17, IFN-γ and IL-4 in $CD4^{+}Foxp3^{+}YFP^{-}$ and $CD4^{+}Foxp3^{+}YFP^{+}$ cells from the spleen of $Cdc42^{fl/fl}Foxp3^{YFP\text{-}Cre/+}$ mice. (**E**) Expression of Foxp3 (MFI) in $Foxp3^{+}YFP^{-}$ and $Foxp3^{+}YFP^{+}$ cells from the spleen of $Cdc42^{fl/fl}Foxp3^{YFP\text{-}Cre/+}$ mice. (**F**) Expression of the indicated Treg functional markers on $Foxp3^{+}YFP^{-}$ and $Foxp3^{+}YFP^{+}$ cells from the spleen of $Cdc42^{fl/fl}Foxp3^{YFP\text{-}Cre/+}$ mice. Numbers indicate MFI. (**G**) Bone marrow cells from $Cdc42^{+/+}Foxp3^{YFP\text{-}Cre}$ or $Cdc42^{fl/fl}$ $Foxp3^{YFP\text{-}Cre}$ mice were mixed with bone marrow cells from BoyJ mice at 1:1 ratio and transplanted into lethally irradiated BoyJ mice. Eight weeks later, donor-derived ($CD45.2^{+}$) $CD4^{+}Foxp3^{+}$ cells in the spleen of recipient mice were analyzed for percentages of total $CD4^{+}Foxp3^{+}$ cells and $CD4^{+}Foxp3^{+}$ cells that express IFN-γ or IL-4. n = 4 or 5. Error bars indicate SD. *$p < 0.05$. **$p < 0.01$.

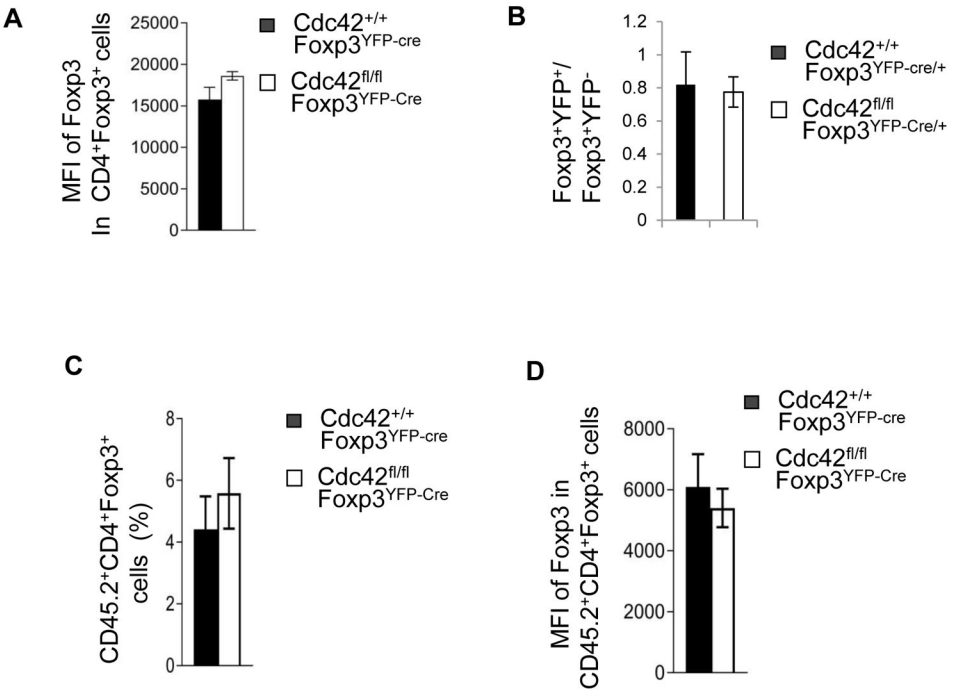

Figure 10.

$Cdc42^{fl/fl}Foxp3^{YFP\text{-}cre}$ mice had impaired thymocyte development but no change in nTreg differentiation. (**A**) Expression of Foxp3 in $CD4^+Foxp3^+$ cells from the thymus of $Cdc42^{+/+}Foxp3^{YFP\text{-}Cre}$ and $Cdc42^{fl/fl}Foxp3^{YFP\text{-}Cre}$ mice. Data are expressed as mean fluorescence intensity (MFI). (**B**) The ratio of $Foxp3^+YFP^+$ vs $Foxp3^+YFP^-$ cells from the thymus of $Cdc42^{+/+}Foxp3^{YFP\text{-}Cre/+}$ and $Cdc42^{fl/fl}$ $Foxp3^{YFP\text{-}Cre/+}$ mice. (**C, D**) Bone marrow cells from $Cdc42^{+/+}Foxp3^{YFP\text{-}Cre}$ or $Cdc42^{fl/fl}$ $Foxp3^{YFP\text{-}Cre}$ mice were mixed with bone marrow cells from BoyJ mice at 1:1 ratio and transplanted into BoyJ mice. Eight weeks later, donor-derived ($CD45.2^+$) $CD4^+Foxp3^+$ cells in the thymus of recipient mice were analyzed for percentages of $CD4^+Foxp3^+$ cells (C) and for Foxp3 expression (MFI) (D). n = 4 or 5. Error bars indicate SD.